Determining the Parameters of Force Curves on *Pseudomonas aeruginosa*: Is "*s*" the Root Spacing or the Mesh Spacing?

A Thesis

Submitted to the Faculty of the

WORCESTER POLYTECHNIC INSTITUTE

in partial fulfillment of the requirements for the

Degree of Master of Science

By

Rebecca L. Gaddis

Date: April 28, 2015

Approved:

Dr. Nancy A. Burnham, Advisor

Dr. Terri A. Camesano, Advisor

Dr. Germano S. Iannacchione, Committee Member

Abstract

Pseudomonas aeruginosa is extremely harmful to immunocompromised individuals. An atomic force microscope was used to measure the surface forces of this bacteria's exopolymers. These forces were characterized with the AdG force model, which is a function of brush length, probe radius, temperature, separation distance and an indefinite density variable, s. This last parameter could represent the root spacing or mesh spacing of the exopolymers. This study aims to clarify s by obtaining force values as a function of temperature. The data suggest that s represents the mesh spacing. If s is the root spacing it should remain constant regardless of the changing polymer lengths, on the other hand if it is the mesh spacing it will vary with changing temperature, as shown by the data presented in this research. This knowledge will aid in understanding and characterizing how bacteria cause infections.

Acknowledgments

This thesis was possible due to the extensive research performed by previous students, the knowledgeable personnel on campus, and my advisors who are so well-versed in this subject area. Special acknowledgments to:

- Past students for their contributions in previous research and analysis development: Samantha O'Connor, Evan Anderson, and Ivan Ivanov
- Lead graduate student in the Laboratory: Lindsay Lozeau
- Primary Physics Advisor: Dr. Nancy Burnham
- Co-Advisor and Principle Professor for the Laboratory: Dr. Terri Camesano
- Committee Member: Dr. Germano Iannacchione

Contents

List of Figures

List of Tables

Chapter 1: Introduction

An area of biological studies that the atomic force microscop (AFM) shows great promise is what has been the study of bacterial adhesion biofilm formation. The AFM allows for study the of bacteria under various conditions without the destruction of the bacteria. This is crucial in developing a cohesive understanding of the mechanics on biofilm growth.

Bacterial biofilms cause many of the persistent infections in the medical community and are a chronic concern for immunocompromised individuals [2]. Biofilms can be generally thought of as communities of microorganisms that adhere to a surface [3]. Although the definition may seem deceptively simple, their composition, structure and cellular organization can become very complex, even to the point where it approaches basic aspects of multicellular life.

Formation of a biofilm begins when the planktonic cells of the bacteria receive environmental signals such as the amount of nutrients, osmolarity, pH, and oxygen levels. The planktonic cells then begin the transition from free-living cells to surface-attached cells. It has been found that the lipopolysaccharides (LPS) of the bacteria are crucial for the attachment process [3].

LPS are found attached to the cell wall of gram-negative bacteria. Lipid A, a product of sugars and hydrophobic fatty acids, anchors the LPS into the cell wall's outer membrane. The core ogilosaccharide, whose composition includes keto-deoxyoctulosonate, and the sugars heptose, glucose, and glucosomine, is attached to Lipid A [4]. The O-antigen, which varies for each bacteria, is the remaining component of the LPS [5].

After attachment a cell's behavior begins to alter. Changes in gene expression, such as down regulation of the gene that produces flagellum, begin to occur. Typically free-living bacteria move via flagellum swimming. However, when the bacteria come into contact with a surface or other bacteria, they begin twitching motility. The pili located on the surface of the cell extend and contract allowing the cell to be pushed or pulled across a surface. Coupled with quorum-sensing molecules, the cells begin to congregate into microcolonies [3].

Quorum-sensing, or cell-to-cell signaling, is a phenomenon that has only recently been discovered and is still being studied. This phenomenon allows gram-negative and positive bacteria to begin to act as a unit rather than as individual cells. It includes the ability to sense cell density and population, as well as signaling other cells within the community [6].

The bacteria also begin to increase production of polymers that form the exopolysaccharide (EPS) matrix of the biofilm. The EPS is an important characteristic of bacterial biofilms, due to its contribution to the antimicrobial resistance of the biofilms. The composition of the EPS matrix depends on the bacteria present, as well as the environment. It surrounds the microcolonies of bacteria, preventing antibiotics from reaching the cells, while allowing for permeable water channels between colonies for the transportation of nutrients and waste to and from these colonies. Figure 1 depicts the individual microcolonies as well as the clear spaces between the colonies referred to as permeable water channels [2, 7].

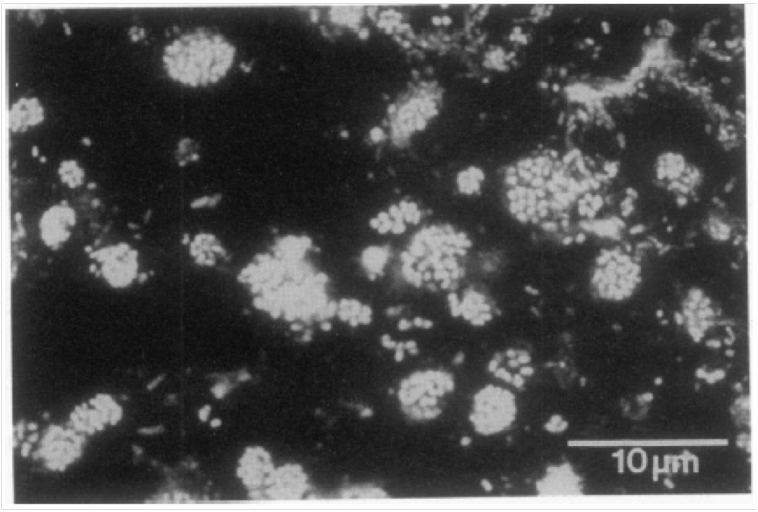

Figure 1: A confocal scanning laser image of a mixed living biofilm from the Bow River in Alberta, Canada. It shows the clusters of microcolonies as well as the clear permeable water channels [2].

Mature biofilms take on a distinguishing mushroom cloud shape. Figure 2 illustrates this shape with *Pseudomonas aeruginosa* PA01 [7]. As a result of detachment signals, such as starvation or overpopulation, detachment can occur. The bacteria can return to the planktonic state to search for other environments such as those rich in nutrients [2, 3, 7].

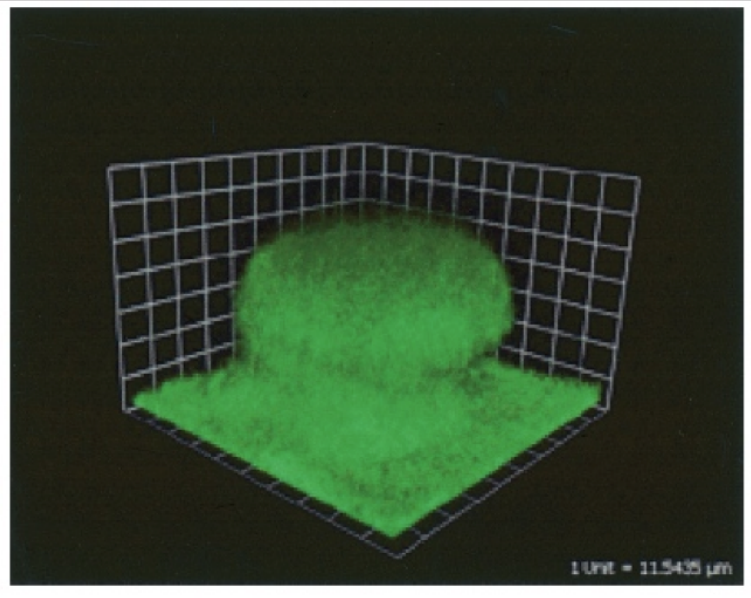

Figure 2: This image depicts the characteristic mushroom shape of biofilms. This image of *Pseudomonas aeruginosa* PA01 was grown in a flow cell reactor [7].

Biofilms can be composed of multiple microbial species or a single microbial species. Typically multi-species are found in nature while single-species dominate the medical community [3]. An intensely studied single-species biofilm bacteria has been the Gram negative, aquatic rod bacterium, *Pseudomonas aeruginosa*.

This bacterium is one of the top five leading causes of nosocomial infections and is one of the most virulent [4, 8]. It can survive in most environments and will form biofilms in any environment that supports growth [3, 6]. This particular bacterium contributes to 30% of pneumonia and septicemia related deaths and 38% of ventilator related pneumonia deaths in intubated patients. It is also associated with a 60% death rate in burn units if an outbreak occurs and a 50% death rate for AIDS patients [6, 8]. This bacterium is commonly found as a biofilm in the lungs of Cystic Fibrosis patients and is especially harmful for these immunocompromised patients [8].

Fighting infections cause by *P. aeruginosa* becomes very difficult due to the serum resistance of the bacteria. In other words, the antibodies and antigens in blood serum are unable

to identify the bacteria. It was found that the LPS of this bacterium contribute to the serum resistance [9].

Treatment of *P. aeruginosa* infections can be challenging due to the antimicrobial resistant nature of biofilms. This bacterium is naturally resistant to many antibiotics and can become multi-drug resistant after failed treatments [6, 10]. It is almost impossible to treat the biofilms found in the lungs of cystic fibrosis patients [6]. Currently many infected patients are turning to the use of viruses that attack bacteria, a treatment known as phage therapy [10].

Since treatment is exceptionally difficult and this bacterium is responsible for a large number of infections and deaths, preventative care would be prudent. However, to administer and create plans for preventative care it is necessary to understand the attachment process of the bacteria, as well as what causes its virulence.

The LPS of *P. aeruginosa* positively correlates with the virulence and has been shown to be vital for the adhesion process. There are twenty types of *P. aeruginosa* that are distinguished by different sets of antigens. These groups are referred to as serogroups. The LPS of this bacterium has the typical composition described earlier with an O-antigen consisting of repeating saccharide units [4, 9, 11]. This heteropolymer B-band is responsible for the distinction between serogroups [4]. However, fourteen of these groups also produce the common antigen or A-band. The A-band, a homopolymer, is composed of approximately twenty-three repeating units of the D-rhamnose sugar polymer [11].

The O-antigen side chains vary in length with different strains of *P. aeruginosa*. The genes Wzz1 and Wzz2 have been identified as the regulators for two different chain lengths [4]. These chains are referred to as long, regulated by Wzz1, and very long, regulated by Wzz2. Chain lengths between 50 and 150 kDa are considered long chains while lengths approaching 250 kDa or more are very long chains [11].

Two particular strains of *P. aeruginosa* have been studied more so than the others. The LPS of strains PA01, of serogroup 05, and PA103, of serogroup 011, have been studied

[4, 11]. Strains within the serogroup 011 are commonly found in infections and have been used in animal models [4]. The Wzz genes were identified first in strain PA01 and were then identified in strain PA103 using the nucleotide sequence of PA01. It was found that Wzz1 of PA103 has 41% identity with Wzz1 of PA01 while Wzz2 has 95% identity [4].

Although the need for two different LPS bands is unknown, speculations regarding the very long chains' connection to serum resistance have been made [4]. The B-band O antigen is much larger than the A-band. Therefore when the B-band is present it covers the A-band. This prevents the antibodies from recognizing the A-band antigens, contributing to the serum resistance [4, 9].

This was further confirmed when mutants of PA103 were compared to the wild strain. The mutant Δ wzz1, meaning the Wzz1 gene was deleted, reduced the inclination for long chain O antigens. The mutant Δ wzz2 resulted in the complete absence of all very long chain O antigens [4, 9]. The Δ wzz1 and double mutant (both genes deleted) both showed decreased survival in diluted normal human serum. However, the Δ wzz2 did not differ from the wild strain indicating that the very long O antigen chains of the B-band are what contribute to serum resistance and therefore the virulence [4].

A technique that has begun to be used to relate the LPS to the virulence of the bacteria has been Atomic Force Microscopy (AFM). The AFM uses a sharp silicon nitride tip whose radius can range between ten and one-hundred nanometers. As the tip approaches the surface of the bacteria, the repulsive steric interactions between the molecules of the tip and surface can be measured. These forces can then be modeled so that the properties of the LPS can be better understood. This technique is also conducive to determining virulent strains of bacteria given that the adhesion is directly related to the virulence [11].

Previous experiments using AFM have characterized the steric forces of the LPS in hopes of better understanding the adhesion process [12]. Alexander and de Gennes have modeled these forces [13, 14]. While most of the variables within the model are well understood, one of the variables has not been clearly defined or characterized. This distance, s, has

been thought to represent the root spacing of the LPS on the membrane [15], yet there is a possibility it actually represents the distance between entanglement points of the LPS.

Using AFM, the steric forces of the mutant ΔWzz1 of strain PA103 have been studied and modeled for this thesis. This deleted Wzz1 gene produces only long LPS chains creating a more uniform distribution of LPS lengths [7]. As the temperature in the system increases, the thermal energy of the system also increases. This increases the LPS fluctuations, thus the layer thickness, L, will change. The hypothesis is that as L changes, the spacing s, of the LPS will also change [15].

The force curves, which are curves produced by the AFM tip and sample interaction showing the force as a function of the tip and sample separation, should reflect these variations due to temperature changes. Therefore, through careful experimentation, the length s can be characterized. If the length s shows a statistically significant variation correlating to the temperature change, it can be concluded that the length s is a representation of the distance between the entanglement points. However, if there is no statistically significant difference between the measurements, then it can be concluded that the length s represents the root spacing.

The remainder of the report will discuss the literature referenced and methods used, as well as data and the conclusions that can be drawn from the data. Each topic will have its own section or chapter labeled as follows, **Literature Review, Methods, Results and Discussion,** and **Summary**. The pages for these specific sections can be found in the table of contents.

Chapter 2: Literature Review

This chapter will focus on necessary information regarding previous research on bacteria and biofilms with Atomic Force Microscopy. Due to the extensive and possibly overwhelming variety of topic in this field, this chapter has been broken down into three major sections. These sections include important aspects of planktonic bacteria, biofilms and more specifically steric forces and the Alexander and de Gennes polymer model.

2.1 Planktonic Bacteria

Planktonic cells are the elementary component to biofilm formation. Thus, much of the current research has focused on individual cells, their components and their characteristics. Bacterial cells contain common characteristics regardless of the strain or type. All bacteria fall into the category of prokaryotes, which are single-celled organisms. Some other common characteristics include, but are not limited to, the lack of a membrane-bound nuclei, the presence of peptidoglycan, plasma membranes, and cell walls [16]. Many studies use the AFM as an imaging method over other common microscopes. Other imaging methods such as traditional microscopes, or electron microscopy, require sample preparation that change or damage the cells. AFM, however, can be executed with live bacteria and does not require staining.

2.1.1 The Membrane

One of the most important characteristics of a microbe has been found to be its membrane. Not only does a membrane maintain the shape of a cell, it transports nutrients, removes waste, and protects the cell and its organelles. There are various structures within or attached to a membrane. Each has its own significance, role and complexity. Understanding those allows us to understand microbes in general.

Many studies have looked at the elasticity of the membrane and have developed models to

characterize the steric forces. However, as reported by Camesano and Logan these models, such as DLVO (Derjaguin, Landau, Verwey, Overneek), do not completely describe these forces [17]. The steric forces of the outer membranes and lipopolysaccharides (LPS) attached to them are very complex.

Schaer-Zammaretti and Ubbink measured elasticity and adhesion of several species of lactic acid bacteria. The group then made a comparison of the species and found that high adhesion forces were observed in species rich with LPS. The strains selected in this research all contained well known and well-defined surface structures and proteins, allowing the research group to relate physical properties with surface structures [18]. Figure 3 depicts the measurements made on *L. johnsonii*.

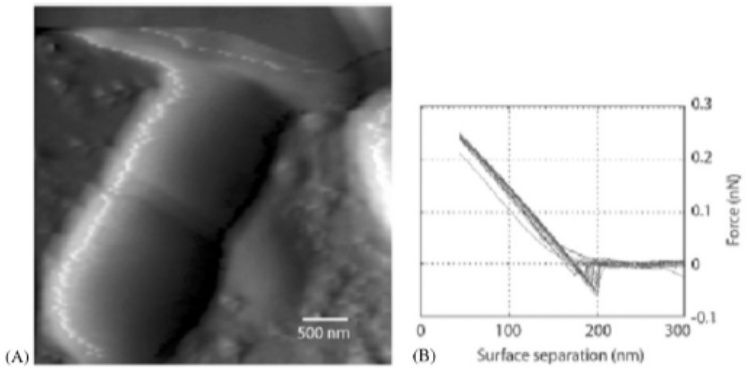

Figure 3: AFM data of *L. johnsonii* ATCC33200: (A) AFM deflection image and (B) Force vs. separation curves depicting several adhesion events [18].

Stoica et al. tried another approach by studying membrane vesicles (MVs) and using a Hertzian model. Gram-negative bacteria have been shown to produce these MVs during a budding process. They determined that not only did the LPS have a role in adhesion to surfaces, but the shape of the MVs also affected the adhesion. When on glass substrates, they found that the MVs change their shape resembling that of a concave lens and demonstrated an elastic force when probed. This indicated that the MVs were under tension creating osmotic pressures on the order of atmospheres. Through force analysis, it was determined that adhesion energies ranged between 6×10^{-6} to 1×10^{-5} $\frac{J}{m^2}$ [19].

2.1.2 Bacterial Stiffness

Using the AFM to study the stiffness of the bacterial surface Longo et al. identified two stiffer locations on all analyzed bacteria. These two features were attributed to stiffer internal components such as DNA. Force topography analyses were performed to better characterize these features. It was found that different stiffnesses were also present within the cell. After the cells were exposed to ampicillin, modifications in the surface properties could be observed, although the topographical structure did not appear to change. The two stiffer features showed a reduced stiffness, while the softer areas of the cells did not change [20]. Although the use of the AFM and force mapping in this study gave a great deal of insight to stiffness changes in *E. coli*, the exact nature of the modifications has not yet been discovered.

Formosa et al. from the National Center of Scientific Research in France has also tested the effects of antibiotics and CX1 (an innovative antibacterial drug) on *Pseudomosa aeruginosa* at the nanoscale using AFM. *P. aeruginosa* also has several multidrug-resistant (MDR) strains requiring new antibiotics with different mechanisms of action. Two antibiotics, ticarcillin and tobramycin, cause cell shape alteration, differences in elasticity and cell wall breakdown. These were compared with CX1 to better understand the mechanism used by this antibiotic [21].

Two strains of *P. aeruginosa* were studied. One of the strains PaR3 was resistant to both ticarcillin and tobramycin while the other strain was not. However, neither showed resistance to CX1. Force curves from the two strains were compared when treated with each of the drugs as seen in Fig. 4. The studied showed that holes were created in the phospholipid bilayer of the gram negative outer membrane.

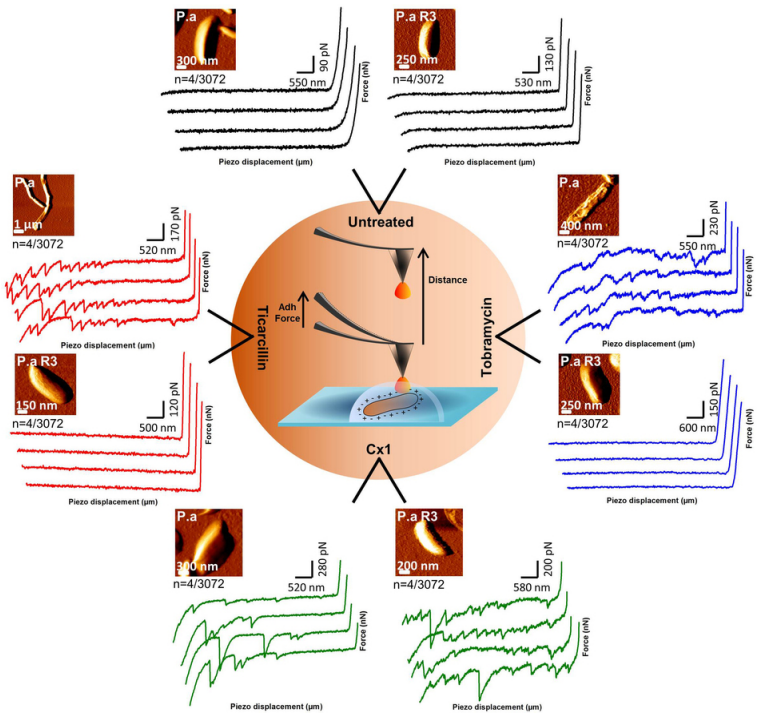

Figure 4: Force spectroscopy comparison schematic of functionalized tips on *P. aeruginosa* $ATCC27853$ and $PaR3$, treated by ticarcillin, tobramycin and CX1). The curves shown depict representative curves of larger data sets. When treated with ticarcillin and tobramycin only $PaR3$ showed resistance. However, neither strains showed resistance to the antibacterial drug CX1 [21].

Formosa determined that CX1 not only disrupted the membrane but damaged the peptidoglycan layer as well. Hypothesis were made that the inner membrane could also have been damaged, although further investigation would be needed for confirmation [21]. Since gram negative bacteria tend to be more resistant to antibiotics, it is very likely that if this antibiotic could penetrate a gram negative membrane it could do the same to the gram positive.

Longo et. al. have utilized the AFM sensitivity, creating a nanomechanical sensor, to detect bacterial metabolism changes in various media and the affects of antibiotics on bacterial metabolism. *Escherichia coli* and *Staphylococcus aureus* were attached to AFM tips via linker molecules in several different experiments. The fluctuations of the cantilever were measured at frequencies below the resonant frequency in phosphate buffered saline, lysogeny broth (LB), and LB with ampicillin. The results showed changes in the fluctuations at the

introduction of the ampicillin for both bacterial strains [22].

Research on the effectiveness of antibiotics remains vital. Each year more and more microbes become resistant to even the strongest antibiotics. The U.S. Centers for Disease Control and Prevention makes reports each year on antiobiotic resistance bacterial threats. In the year 2013 there were reported to be at least $2,049,442$ infections due to drug resistant microbes. Of that large number $23,000$ resulted in death. *Pseudomonas aeruginosa* and *Escherichia coli* are responsible for five prceent of those deaths alone [23].

2.1.3 Lipopolysaccharides

Much of a bacteria's virulence can be connected to the LPS of the outer membrane as determined by Ivanov et. al. [11]. However, only gram negative bacteria have LPS, making them more aggressive and resistant to treatment. The LPS facilitate the bacteria's interaction with the external environment making them responsible for the first step in forming biofilms.

In the youth of the AFM probing LPS or any surface brush was very difficult if not impossible. Air drying samples causes aggregates to form and the AFM tip to stick to the surfaces of the substrates. It was not until intermittent contact mode (IC) had been created, that extensive studies of the polysaccharides could be made [24].

Camesano and Logan were able to measure the forces of LPS on *Pseudomonas putida* and *Burkholderia cepacia* using IC mode. These forces were well modeled by the electrosteric repulsion model, which allowed equilibrium brush length of the LPS to be measured as a function of pH and ionic strength. Figure 5 illustrates force curves and the steric repulsion model used to fit them.

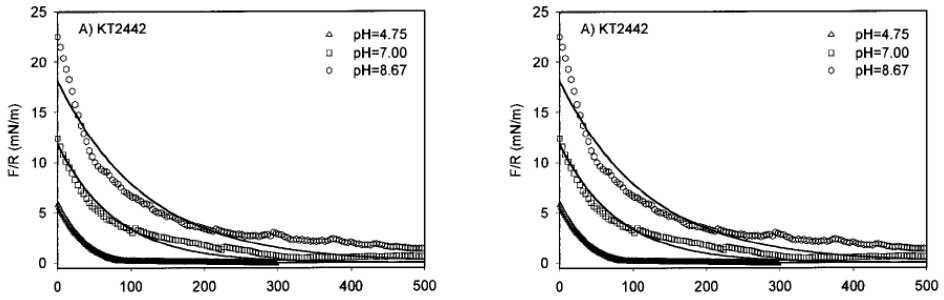

(a) *P. putida* (b) *B. cepacia*

Figure 5: Some examples of the steric repulsion model used to fit AFM force data, shown for (A) *Pseudomonas putida* KT2442 and (B) *Burkholderia cepacia* G4 as a function of pH at 1 mM [17].

Intermittent contact mode also allowed the use of functionalized AFM tips. Gad et. al obtained images of polysaccharides using a technique called force volume imaging in the late $1990's$. This technique used a functionalized tip containing a receptor protein to identify its target molecule (polysaccharide ligand) on a substrate. Force curves were obtained and the forces measured, to identify the locations of binding. This method, however, showed some limitations. Ideally only one receptor protein should be attached to the AFM tip to acquire clear and accurate force measurements, but to do this in practice is almost impossible [25].

A similar study was done using a functionalized AFM tip containing concanavalin A lectins. Using this method, polysaccharides on live cells were stretched. Chemical nature, surface distribution and extension could all be characterized using this method referred to as SMFS (single molecule force spectroscopy) [26].

The structure of the LPS can be very complex depending upon the bacteria. However, the general structure consists of a hydrophobic lipid A region, followed by a core oligosaccharide (inner core and outer core) and finally a repeating polysaccharide (O-antigen) that varies in length [27]. Figure 6 depicts this general structure.

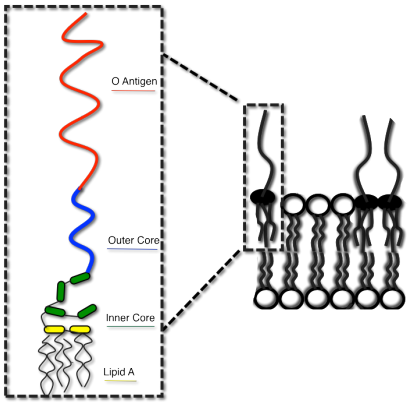

Figure 6: Schematic structure of LPS.

The O-antigen has been studied for various bacteria. Since the LPS play a crucial role in the bacteria's survival and ability to infect, it is important to understand their structure, sensitivities, and resistance. Many studies have been done focusing on the O-antigen regulation, specifically regulation of this antigen in *Pseudomonas aeruginosa* [9, 4]. The O-antigen is also used to determine strains of a particular bacteria due to the variable components in the LPS [28].

It was discovered that a specific, transmembrane helix gene, (Wzz), regulates the O-antigen chain length in gram negative bacteria [29]. Hull's group was the first to report this regulation gene. They determined that the Wzz gene regulates the polymerization process. This polymerization process is very similar to that of capsular polysaccharides in both gram negative and positive bacteria [30].

Kintz and Goldberg determined that these O-antigens could be affected in two different ways by outside factors; the amount attaching to the lipid A or the length to which the antigen will grow. For instance, the very long chain length regulated by Wzz2 in *Pseudomonas aeruginosa*, is much more susceptible to environmental changes than the long chain regulated by Wzz1. Despite what Kintz and Goldberg discovered, much of the connection between Wzz genes and the O-antigen chain lengths needs further investigation [9, 4, 11].

Although the Wzz genes regulate the length of the LPS, it is difficult to get an actual

value for that length through chemical analysis. Western blots can give an idea of relative lengths as well as atomic mass, but through force curves on the AFM, numerical lengths can be obtained [11, 31].

While measuring the steric forces on the surface of the bacteria, the AFM obtains a force curve. That curve can then be fit to a model depending upon the interactions. Models such as the worm like chain, Aledander and de Gennes, DLVO, and electrosteric models are used frequently. These models have a brush length parameter for which a value can be measured when fitting the force curve. The length of the LPS depends upon the length of the O-antigen, which varies across the bacteria [11]. Although this method does not produce exact values for various O-antigens it does produce the equilibrium brush length of the LPS.

The LPS, or more specifically the O-antigen, has been known to change composition during different steps of the biofilm formation process. The presence or absence of this antigen greatly affects the toxicity and virulence of the bacteria. The absence of the O-antigen has some correlation to a process many gram negative bacteria utilize to inject toxins into host cells. This process is referred to as type three secretion system [32, 33].

Augustin et. al hypothesized that the presence of the O-antigen on *Pseudomonas aeruginosa* would aid the cytoxicity process, however it was discovered that the absence of the O-antigen actually may send a signal to increase TTSS expression. The O-antigen's composition quickly and significantly changes from planktonic cells to cells in biofilms [27]. More studies need to be done to better understand how the O-antigen composition and TTSS expression link to the biofilm formation process.

2.1.4 Bacterial Motility

Many, though not all, bacteria exhibit self propelled motion, referred to as motility. This includes but is not limited to swimming, swarming, gliding, twitching and sliding. Though some of the mechanisms by which the bacteria move are not known, flagella are very important to most of the observed bacterial motility. In the last few years studies have

been done using the AFM to observe various types of motility and what changes the bacteria exhibit while undergoing this movement.

Dhahri et. al. have studied the non-motile *Rhodococcus wratislaviensis* and motile *Nostoc* bacteria. Both bacteria produce a polymeric slime which was studied to test the hypothesis that *Nostoc* uses the ejection of slime to move. The gliding mechanism is one of the types of movement that is the least well understood. However, this research used an AFM to measure the thickness of a polymeric slime left by both strains and examined the characteristics of the slime. The thickness of the non-motile bacteria was greater than that of the motile bacteria, which was attributed to the adhesion and gliding speed of the bacteria respectively [34].

Gillis et. al. , on the other hand, studied swarming motility of *Bacillus thuringiensis sv. israelensis*. The amount of flagella and cell morphology in cells harvested from the edges and centers of colonies was examined. The group used an AFM to observe cell arrangement, shape and amount of flagella present. The study showed cells taken from the center of the colony to be non-flagellated, rod-shaped and arranged in chains [35]. In Fig. 7, the more flagellated cells from the rim of the colonies have been shown. Individual flagella can be observed.

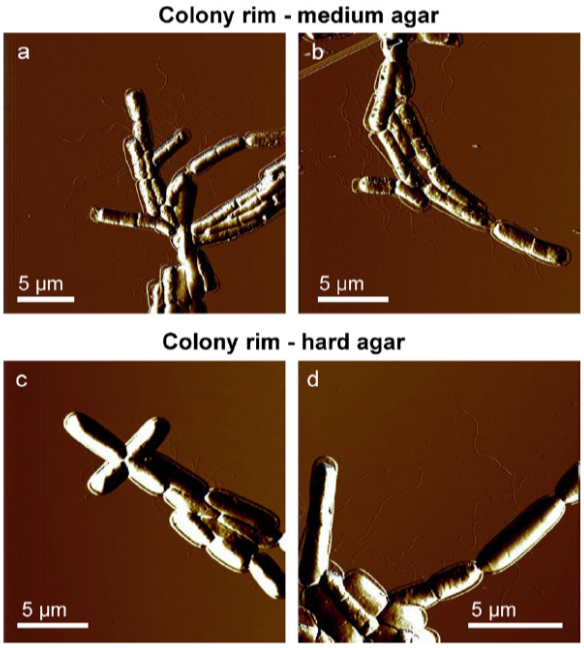

Figure 7: Nanoscale surface structure of colony-rim cells grown on medium and hard agar. (a–d) Deflection images recorded in air for *B. thuringiensis sv. israelensis* cells harvested from the rims of colonies grown on (a, b) medium agar and (c, d) hard agar. Individual flagella can be seen [35].

2.1.5 Adhesion

Although the LPS and EPS are both responsible for bacterial adhesion they are not the only factors that influence adhesion. Bacterial properties and surface properties both influence the process. Hydrophobicity, and zeta potential are properties of both the bacterial and substrate that are influential. Motility, LPS and EPS are bacterial properties while surface texture is a substrate property [36, 37, 38]. It has been found that even differences in medium can greatly impact the adhesion of bacteria. *Escherichia coli* biofilms have been found to develop faster in low nutrient medium and become more adhesive as they matured [39].

Through AFM force curve analysis a great deal of information regarding the adhesion of the bacteria can be gained. This allows studies to identify which of the properties are more influential for different bacteria. For instance, Astrid Roosjen et. al. determined that cell surface hydrophobicity is caused by LPS and biosurfactants [36, 40].

Force curves contain a plethora of information, more so when both approach and retraction curves are analyzed. Approach curves on bacterial surfaces provide information regarding the LPS structure. Retraction curves provide information on the strength of the adhesion. Figure 8 shows approach and retraction curves for *P. aeruginosa* strains AK1401 and PAO1 [41].

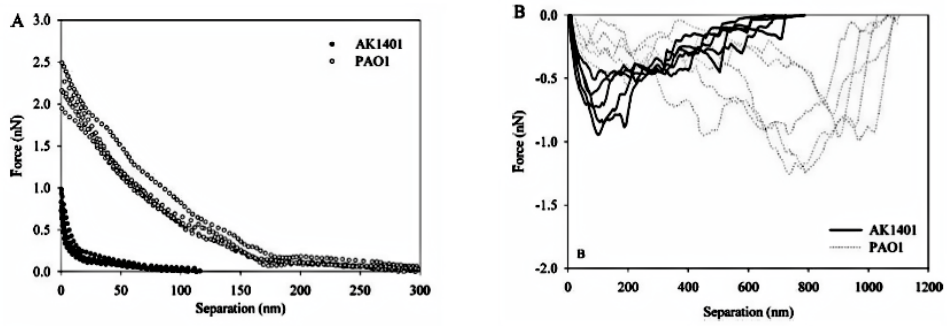

(a) Approach Curves (b) Retraction Curves

Figure 8: Representative AFM (8a) approach and (8b) retraction curves of *P. aeruginosa* strains $AK1401$ and $PA01$. Five data sets that represent typical data obtained for five bacteria are shown. In total, 10 bacteria were examined per condition, and five measurements were made over the center of each cell [41].

An increasingly popular method of measuring bacterial adhesion is one in which the AFM tip is functionalized with the bacteria and a substrate is approached. Rather than studying the approach of a AFM tip onto immobilized bacteria, many studies have begun immobilizing the bacteria to an AFM tip and approaching various surfaces. Ovchinnikova et. al. attached *Staphylococcus aureus* to an AFM tip and approached *Candida albicans* to measure the variation in adhesion of *Staphylococcus aureus* along *Candida albicans* [42].

Many other studies conducted compare the adhesion of various bacterial to different surfaces such as aluminum as was done by Sheng et. al. [43]. Touhami et. al. used *Pseudomonas aeruginosa* functionalized AFM tips and a mica substrate to determine the importance of type IV pili in bacterial adhesion [44]. Still many studies simply use the AFM to characterize the adhesion forces of specific bacterial strains. Volle used this technique to characterize the

adhesive forces of five different bacterial strains and a silicon nitride AFM tip [45].

2.2 Biofilms

Although microbiology has been a designated branch of biology since the late seventeenth century, it has only been within the last few decades that microbial biofilms have been studied extensively [7, 46]. The American Society for Microbiology (AMS) has sponsored a series of conferences dedicated to biofilms since 1996 [7]. These conferences began after their 1993 annual meeting and they allow all disciplines interested in biofilms to communicate results.

At the 1993 annual meeting, Costerton and five others presented data on biofilms that deemed the subject worthy of four-day conferences. Costerton et al. reported the use of confocal scanning laser microscopy to determine that biofilms were not homogeneous as previous thought. Confocal scanning laser microscopy was also used to determine the basic form of the biofilm; permeable water channels within an exopolysaccharide (EPS) matrix surrounding small but dense microcolonies [2].

Using microelectrodes with confocal scanning laser microscopy the dissolved oxygen within the biofilm of *P. aeruginosa* was studied. From these data the convection flow within the permeable water channels was clearly seen. A remarkable discovery related to the dissolved oxygen explained how aerobic and anaerobic species could live within the same biofilm. It was found that as the probe reached the center of the microcolony the levels of dissolved oxygen decreased and increased outside of the colonies. These data can be seen in Fig. 9.

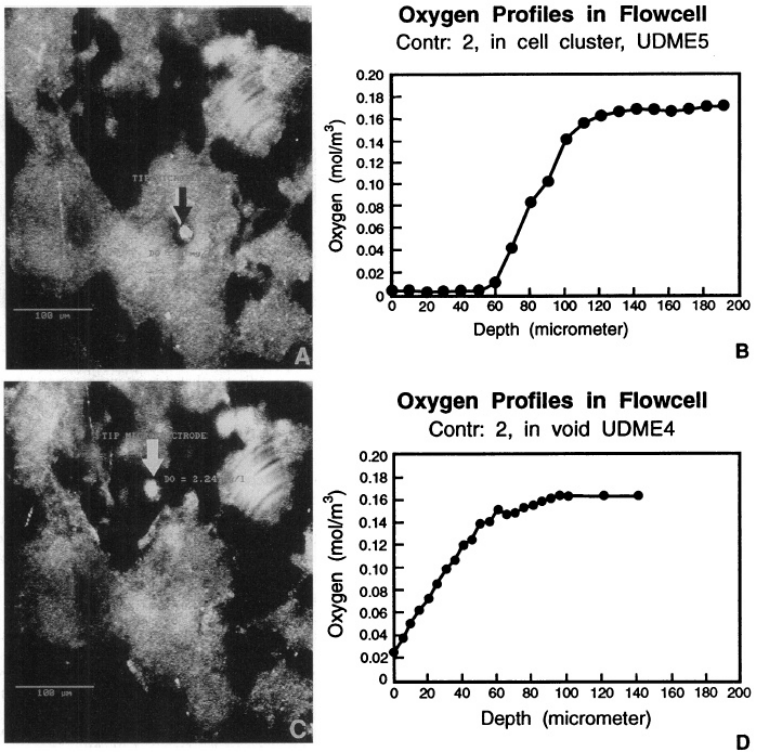

Figure 9: Confocal scanning laser micrographs (left) and dissolved oxygen data (right) obtained with microelectrodes for *P. aeruginosa*. The dissolved oxygen probe was moved from the bulk fluid into the center of the microcolony and back to the bulk fluid taking readings at regular intervals. The data indicated that the water channels trasport dissolved oxygen. The arrows indicate the position of the probe [2].

Several groups presented information on interspecies interactions at one of the conferences hosted by AMS. Hentzer from the department of Molecular Microbiology at BioCentrum-DTU in Denmark, studied the interactions of *P. aeruginosa* and *Burkholderia* in cystic fibrosis lung infections [7]. Dunn had determined through screening that *Sinorhizobium meliloti* uses similar factors as tomato plant roots to colonize abiotic surfaces [2].

There were also impressive displays of research techniques introduced at the 2003 conference. Wagner utilized advanced techniques such as Fluorescence In Situ Hybridization used in cytogenetics, microsensors, and microautoradiography-stable isotope probing to determine the resolution of individual species and phylogenetic groups, metabolic activity, and profiles of chemical gradients within the biofilm [7]. Whiteley addressed the difficult task of

evaluating gradients of gene or protein expressions in specific systems. He applied a variation on a technique that identifies virulent genes while studying *P. aeruginosa* PA14. This technique was considered a new genetic tool at the 2003 conference [7].

One of the extensively studied biofilm bacteria has been *P. aeruginosa* largely due to its association with high death rates in immunocompromised individuals. Christian Delden and Barbara Iglewski from the University of Rochester School of Medicine and Dentistry have reported that cell-to-cell signaling, or quorum-sensing, is directly related to the virulence of this bacterium. Delden and Iglewski describe two cell-to-cell signaling systems for *P. aeruginosa*, the *las* system and *rhl* system. These systems were named according to the genes regulated and produced within the systems. It was found that the *las* system is involved in the development and maturation of *P. aeruginosa* biofilms [6].

Other genetic studies such as those done by Wozinak and colleagues have shed light on the complex process crucial to biofilm formation in which the bacteria adhere to various surfaces. Wozinak's laboratory has shown that surface attachment regulates genes within *P. aeruginosa* that are responsible for the production of flagella and alginate. Flagella are vital to the motility of the bacterium while alginate has been found in the EPS matrix of the biofilms. Wozinak showed that on surface contact flagellar synthesis slows, while alginate synthesis is increased [3].

2.2.1 Biofilm Surfaces

Although biofilms are composed of many individual bacteria, properties of biofilms can be very different from those bacteria. Rather than simple well known shapes and sizes, bacterial biofilms can be very complex in shape, size and composition. The structure of a biofilm can drastically change depending on the environment or bacterial strains involved in its formation. For example, *Pseudomonas aeruginosa* can form a flat, very active biofilm or a heterogeneous mushroom-shaped biofilm with many colonies and permeable water channels [47].

Biofilm coverage can be determined by AFM imaging. This may be important for studies involving biofilm adhesion or corrosion, which are discussed further in the following sections. Imaging with the AFM can also be used to confirm the presence of biofilms or substances they secrete before other analysis is done. For example, P. Lal et. al. used an AFM to obtain images and dimensions of *Candida albicans* biofilms to help identify extracellular polymeric substance (EPS) production [48].

The topographical images obtained via the AFM can also help determine the effect of different substrates on biofilm formation. Oh et al. used images obtained via an AFM to compare the effect aluminum, steel, rubber and polypropylene had of the formation of *Pseudomonas aeruginosa* biofilms [49]. The AFM images depicted surface morphology differences of the biofilm grown on the different substrates as seen in Fig. 10.

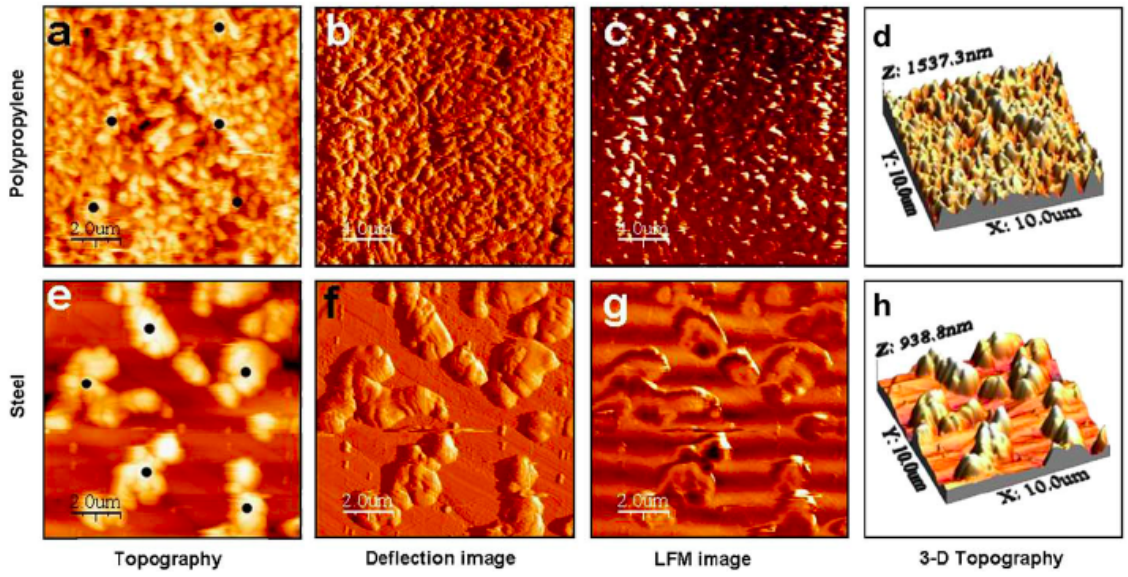

Figure 10: AFM images of biofilm, which was grown for 3 days on steel and polypropylene: topographic, deflection, LFM and 3-D topographic images of the biofilm on (a-d) a polypropylene surface, and (e-h) a steel surface are shown. All the images show an area of $10 \times 10\ \mu m^2$. Significant differences between the biofilm growth can be seen between the two substrates[49].

2.2.2 Extracellular Polymeric Substance

The LPS layer or brush layer is responsible for cell-cell interactions, cell migration and the adhesion of the bacteria to surfaces. Analysis of force curves from an AFM can help detect brush layers on bacteria, as well as determining some of the characteristics of those layers [31]. AFM analysis can also help determine the type of polymers necessary for biofilm formation of various bacteria.

When bacterial cells first attached to surfaces it is considered non-permanent or reversible attachment. However, biofilm growth begins when that reversible attachment becomes permanent attachment. At this stage the cells begin to form the EPS or extracellular polymeric substance. Studies have shown that EPS inhibits the initial attachment of the bacteria yet is vital to the growth and structure of the biofilm. For instance, Gómez-Suárez et al. found that initial adhesion instances and rates as well as redeposition rates were greater for non-EPS-producing *Pseudomonas aeruginosa* compared to EPS-producing *Pseudomonas aeruginosa*. After detachment the EPS-producing bacteria left a thick and irregular EPS layer detected by AFM [50].

Pseudomonas aeruginosa produces three extracellular polysaccharides, alginate, Psl and Pel. The significance of the polysaccharides in biofilm formation greatly depends on the strain of *P. aeruginosa* used. For instance, in the strain PAO1 Pel and alginate do not contribute greatly to biofilm development while Psl does. However, in some strains of *P. aeruginosa* Pel maintains cell to cell interactions and provides the biofilm protection from antibiotics [51, 52].

Since these polysaccharides are responsible for cell to cell interaction and adhesion of the cells, the AFM can be used to measure steric forces as well as forces of adhesion providing insight into the exact role of the polysaccharides. Many studies use this method and compare the forces between various strains and mutations. The comparison between mutant provides insight into which polysaccharide is dominant in which strain.

Benjamin Cooley et. al. used AFM force measurements to determined that *P. aeruginosa*

strains which lack pili, Pel not only contributes to intercellular cohesion and protection but is vital to cell attachment. Cooley compared force curves on various locations of individual bacteria as well as individual mutated bacteria. The measurements indicated that Pel was important for symmetric attachment of bacteria; meaning without Pel cells lacked the ability to become flat and permanently attach to surfaces [52].

Although Pel plays a role in *P. aeruginosa* colanic acid, cellulose and PGA are thought to influence biofilm development for *E. Coli*. These polysaccharides provide shape, support and protection for the Biofilm. Several studies with the AFM have been done on colanic acid's role in the biofilm development [53].

Hanna et. al. used the AFM to study the physiochemical and specific binding interactions of *E. Coli*. The results in this study indicated that colanic acid did not improve bacterial adhesion and in fact blocked specific binding. They suggested that *E. Coli* did not express colanic acid until after adhesion and during the development of mature biofilms [54]. On the other hand, Razatos et. al. reported that electrostatic interactions were found to dominate the adhesive behavior of *E. Coli* strains that overproduced colanic acid [55].

2.2.3 Biofilm Adhesion

Due to the mutlicellular nature of biofilms the properties of biofilms can be very complex. An important aspect of biofilm growth is the detachment phase. In this stage of the development the biofilm relases some cells to migrate and start the process mentioned in the introduction again. Therefore cohesive strength is vital to the detachment and growth phases. Ahimou et al. studied the cohesive strength of heterogeneous biofilms obtained from a wastewater treatment plant, using the AFM. Using frictional force images and measurements the cohesive energy was calculated. A comparison of cohesive energy when calcium was added showed an increase of approximately five percent [56].

Although biofilm formation begins with the adhesion of a single bacterium, biofilms also display properties of adhesion. Studies on biofilm adhesion have provided insight into the

adhesion at different stages in biofilm development as well as how some mutations may change these properties. Some of these studies have used microbead force spectroscopy to study the adhesive nature of biofilms. P. Lau et. al. attached a 50 μm diameter glass bead to the bottom of a tipless cantilever. *Pseudomonas aeruginosa* strain PA01 and the mutant strain wapR were grown on different microbead tips, developing into biofilms. Figure 11 shows a scanning electron micrograph of the biofilm on the glass bead [39].

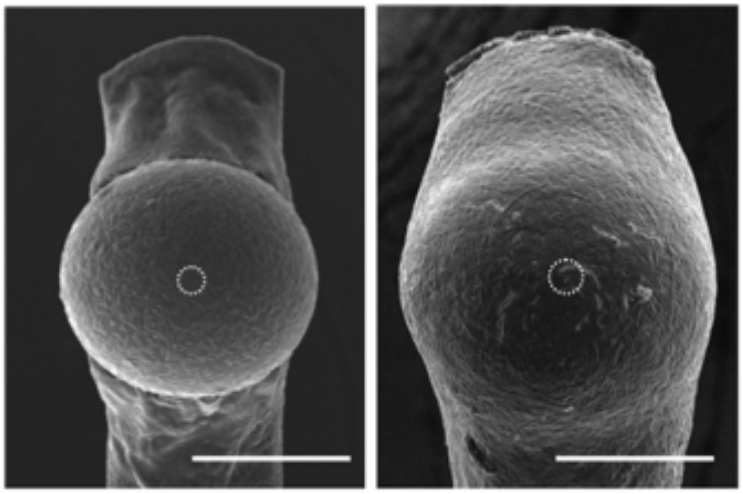

Figure 11: Bacterial biofilm-coated glass beads used in microbead force spectroscopy. The study showed that the adhesion for early biofilms (left) was greater that mature biofilms (right). Typical area of contact is indicated by the white dashed circle at the center of each image [39].

The study showed that early biofilms were more adhesive than mature biofilms for both PAO1 and wapR. Interestingly the wapR showed greater adhesive properties. The wapR mutant has truncated LPS lacking the O-antigen. The study also compared contact time, loading force, and retraction velocity, finding the significance of these factors to decrease respectively [39].

2.3 Steric Forces and the AdG Model

These polymers, however, are not the first to be studied, scaled, or characterized. Alexander and de Gennes first described the force interactions between polymer brushes in the

nineteen seventies and eighties. Alexander determined the first relationships between the Helmholtz free energy, stretching energy, and the chain parameters of each polymer chain [13].

Several years later de Gennes expanded Alexander's relationships creating what is now known as the Alexander and de Gennes, or AdG, model for steric forces of polymers at an interface [14]. He, unlike Alexander, made a distinction between types of polymer adhesion. While Alexander's model contained a characteristic length parameter, the modified de Gennes' version concluded that the length parameter s, represented the root spacing of the polymers for physically attached polymers of a single layer and the mean distance between entanglement points (mesh spacing) for terminally attached chains.

The AdG model then took the form of Eq. 1 as seen in the modeling presented by Debby Chang et al. for describing the steric forces and interactions of lubricin and hyaluronic acid on substrates [12]. Chang noticed that adhesion of the lubricin onto the probe decreased with scan speed and increased with contact force and longer dwell time. The force model or a spherical tip

$$F(D) = \frac{8\pi k_B T R L}{35 s^3} \left[7 \left(\frac{L}{D} \right)^{\frac{5}{4}} + 5 \left(\frac{D}{L} \right)^{\frac{7}{4}} - 12 \right], \tag{1}$$

is a function of temperature T, separation D, tip radius R, layer thickness L, and an ambiguous density parameter s.

Soon after de Gennes modified the model, Hillary Taunton and colleagues studied the interactions between surfaces with end-adsorbed chains [57]. Their focus was on chains that were physisorbed rather than chemically bonded to the surfaces. The group specifically sought systems that contained nonadsorbing chains with a single polar functional group at one end that would adhere to the substrate surface. The two systems they used were polystyrene chains with carboxyl and n-dimethyl terminal groups as well as poly(ethylene

oxide). Using the AdG model Taunton calculated a mean spacing distance between grafting points of the polymers of 85 Å and a layer thickness of approximately 740 Å.

Hans-Jürgen Butt and colleges used the AFM and a stage heater to measure the steric forces of polystyrene in cyclohexane and poly(ethylene oxide) as a function of temperature [15]. Butt used the grafting density to determine the mean distance between grafting sites to be approximately 4 nm. It was also determined that the steric forces and consequently the layer thickness increased monotonically as temperature increased within the range of $10 - 70°$ C. This result can be seen in Fig. 12. Two force curves are shown in Fig. 12a to compare the force differences observed at two different temperatures, 35° C and 52.5° C. The monotonic relationship between the layer thickness and temperature is represented in Fig. 12b. There were different range components, corresponding to different values of the equilibrium thickness, which lead to different exponentially decaying functions used to fit the retraction of the force curves.

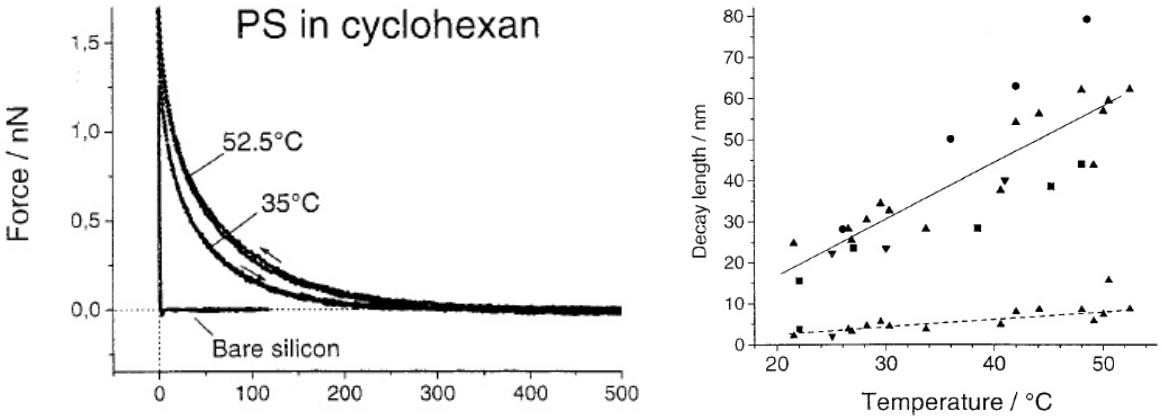

(a) Force Curve **(b)** Decay Length

Figure 12: (A) Force curves of polystyrene grafted to silicon as a function of temperature. (B) Temperature dependence of decay length (layer thickness) for long-range component (solid line) and short-range component (dashed line) [15].

At the University of Bielefeld, Serr used force spectroscopy to characterize the interaction forces of poly(styrene-4-sulfonate)-covered surfaces [58]. He used the AdG model and

observed extremely strong adhesion forces on retraction of the probe. The force curves were taken as a function of ionic strength with a specific molality of sodium chloride. They were also taken from increasing ionic strength as well as from decreasing ionic strength. Figure 13a and 13b show the resulting force curves at AdG fits for 0.2 M of sodium chloride and 1 M of sodium chloride, respectively.

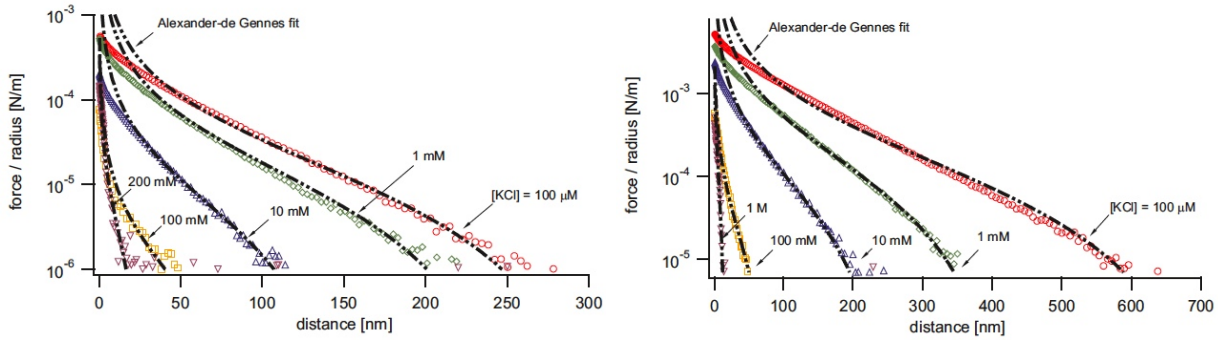

(a) 0.2 M **(b)** 1 M

Figure 13: Force curves of poly(styrene-4-sulfonate) in a (a) 0.2 M KCl solution and (b) 1 M KCl solution [58].

Figure 14a shows the computed values for the layer thickness L, and according to Serr, the mean distance between attachment points, s. Fig. 14b compares the values of L and s obtained from reversing the direction of ionic strength from increasing to decreasing. Much of the previous work can be conceptually and even mathematically applied to the steric forces of the LPS on bacteria. The LPS are crucial for adhesion of the bacteria onto surfaces, making them the focus of many experiments.

ionic strength [M]	theoretical κ^{-1} [nm]	PSS 0.2 M[a] L [nm]	PSS 0.2 M[a] s [nm]	PSS 1 M[b] L [nm]	PSS 1 M[b] s [nm]
1	0.3			8	16
$2 \cdot 10^{-1}$	0.7	14	65		
10^{-1}	1.0	50	145	42	48
10^{-2}	3.0	75	85	123	41
10^{-3}	9.6	125	76	205	40
10^{-4}	30.4	150	75	350	48

(a) 0.2 M

ionic strength [M]	high → low [KCl][a] L [nm]	high → low [KCl][a] s [nm]	low → high [KCl][b] L [nm]	low → high [KCl][b] s [nm]
10^{-1}	50	145	29	46
10^{-2}	75	85	60	42
10^{-3}	125	76	90	36
10^{-4}	150	75	84	39

(b) 1 M

Figure 14: Values of L and s obtained from force curves of poly(styrene-4-sulfonate) (A) in a 0.2 M KCl solution and 1 M KCl solution (B) and moving from a high ionic strength to a low ionic strength and vice versa [58].

Mildred Rivera has also analyzed the chain length of the LPS [59]. Rivera's and Kintz's groups utilized chromatography and western blotting to determine these chain lengths for PA103 and its mutants. Long chain lengths are between 50 and 150 kDa while very long chain lengths are approximately 250 kDa [11].

Understanding the composition and size of the LPS becomes important when the LPS characteristics can be related to the virulence of the bacteria. Ivan Ivanov and Erica Kintz related the properties of the LPS to the virulence using Atomic Force Microscopy [11].

Ivanov and Kintz determined that as the LPS length increased the repulsion force within the AFM also increased. The experiments also showed that the bacteria that contained only the shorter LPS on the cell wall behaved similarly to stiff samples. The addition of long LPS chains smooths the repulsion forces. This can be seen in Fig. 15 [11].

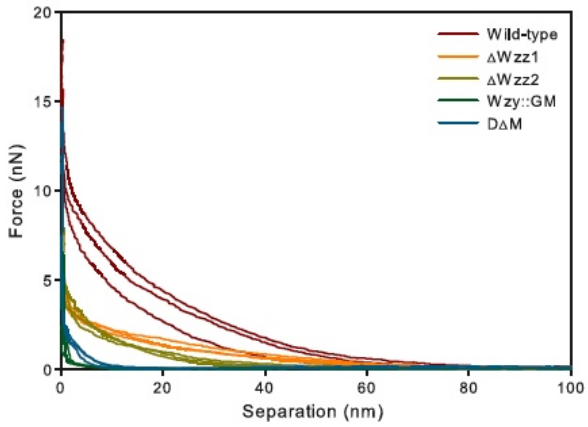

Figure 15: Repulsive AFM force curves of *P. aeruginosa* PA103 wild-type and mutants. ΔWzz1 has only long chains, ΔWzz2 has short chains and Wzy::GM is a double mutant with no chains [11].

Using the AdG steric model, Ivanov and Kintz modeled the spacing of the LPS. The smallest observed spacing was found in the wild-type strain at less than 4 nm. The largest observed spacing was found in the Wzy::GM mutant at almost 16 nm. The Wzy::GM mutant was the experimental control, a mutant of PA103 with the LPS core and only one subunit of the o-antigen. The LPS of this mutant were the shortest in chain length. The results of the spacing can be seen in Fig. 16.

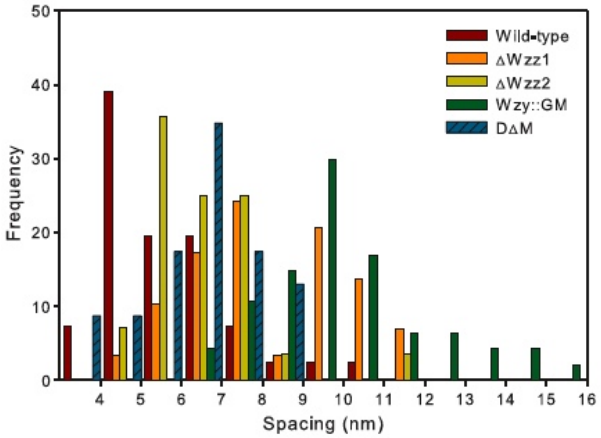

Figure 16: Spacing of LPS determined using the AdG model, PA103 wild-type and mutants [11].

Atabek and Camesano used AFM to study the effect of lipopolysaccharides on the ad-

hesion of *P. aeruginosa* PA01 and AK1401. They analyzed both the approach and the retraction of the force curves obtained from the different strains. The approach provided information on the steric forces of the bacteria's surface, which can be seen in Fig. 17a. The retraction, however, provided information on the adhesion strength of the LPS [41].

An interesting incident that occurred on retraction curves were "pull-off events", which represented the point at which polymers that had been attached to the AFM probe broke away from the tip. Figure 17b depicts these events for both strains of *P. aeruginosa*. The local minima on each curve, referred to in the paper as "adhesion peaks", represent the unfolding of the chains of the LPS when the curve does not return to zero and the breaking point otherwise.

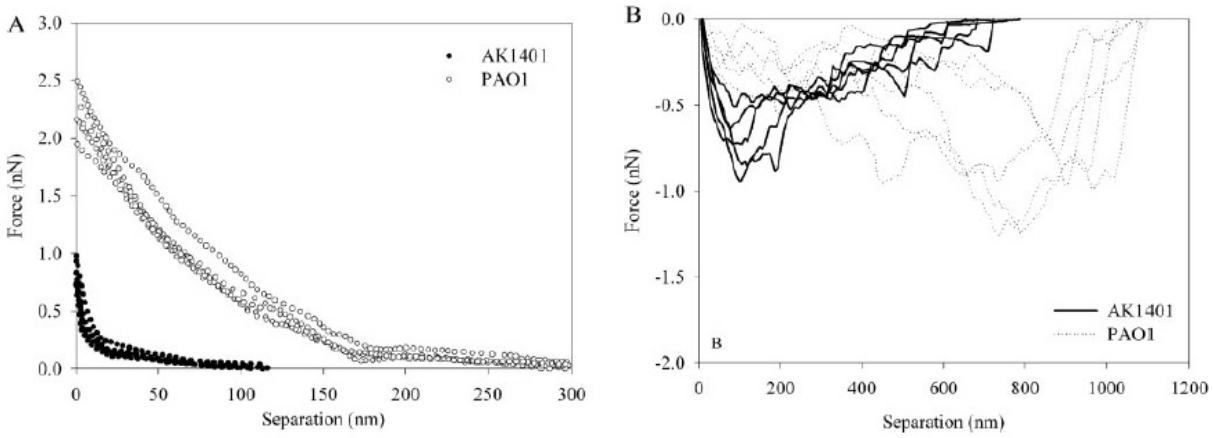

(a) AFM Approach **(b)** AFM Retraction

Figure 17: (a) The AFM approach and (b) retraction curve obtained from PA01 and AK1401. These were typical force data obtained from five bacteria of which five measurements were taken on each [41].

Although many have analyzed the steric forces of polymers using the AdG model, the studies have primarily been done with grafted polymers. However, polymers that have been terminally grafted to substrates have similar restrictions to those of the LPS on bacteria. Therefore, as de Gennes distinguished, the expected values of s should fluctuate with L as the mesh spacing rather than the root spacing. It is expected that as the temperature of

the sample increases, L will increase, as will s. L should remain below several hundred nanometers and s is not expected to greatly exceed L at any point.

Chapter 3: Methods

Due to the detail and number of steps in the procedure and analysis, this chapter has been divided into several sections. These sections include ***Pseudomonas aeruginosa* Growth and Preparation**, **Atomic Force Microscopy**, and **Analysis**.

3.1 *Pseudomonas aeruginosa* Growth and Preparation

A procedure developed in Camesano's lab at Worcester Polytechnic Institute's (WPI) Life Sciences and Bioengineering Center was used to prepare the samples for AFM imaging. Evan Anderson, a physics graduate student at WPI, developed the basis of the sample preparation procedure found in Appendix A [60].

The *Pseudomonas aeruginosa* (PA103) was initially grown from stock then plated onto Luria-Bertani (LB) agar, which was then used in growing cultures for future experiments. The agar plates lasted approximately thirty days after which the bacteria were too old to use. They were grown in fifty milliliters of LB broth for approximately twelve to sixteen hours in an incubator or until the adsorbance reached at least 0.7 AU and at most 1 AU. Members of Professor Terri Camesano's lab used spectrophotometry to determine the time of growth for these bacteria. At approximately twelve hours the bacteria is within the exponential phase of its growth. This phase is indicated in Fig. 18 by the label. Although this figure is a general diagram of bacterial growth the concepts of the phases are the same.

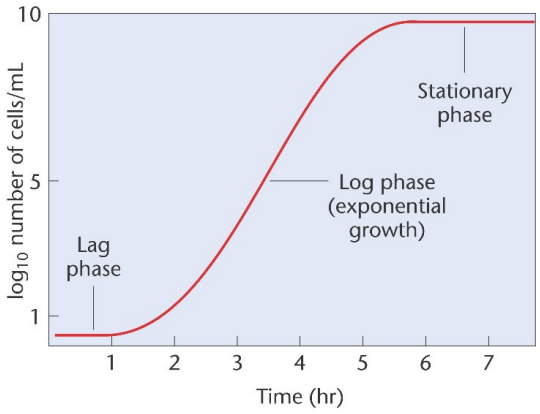

Figure 18: Schematic of the exponential growth phase of bacteria indicated by the label. The graph is a general growth curve and not specific to PA103.

Clean glass slides are necessary for the sample preparation as they are the substrate to which the bacteria will bind. The glass slides were sonocated in 2% RBS solution for ten minutes. The glass slides were then thoroughly rinsed in deionized water then with ethanol. For a more detailed procedure refer to Appendix A.

Once the bacteria have been grown and are ready for the adhesion process ten milliliters of bacteria is poured into two centrifuge tubes. The bacteria is centrifuged three times and washed with clean water in between each centrifuge. Clean water is high quality water with no pathogens, bacteria, or contaminents. This differs from Ultra Pure water or milliQ water, which has been passed through complex filters to decrease conductivity and extract ions. For specific steps and centrifuge time and spin levels, see Appendix A.

While the bacteria are in the centrifuge, the clean glass slides are soaked in a 1 to 2.3 ratio of 3-aminopropyltrimethoxysilane (Aminosilane) and methanol in a petri dish for twenty minutes. After the final centrifuge cycle the bacteria in the tubes are combined leaving approximately ten milliliters in one centrifuge tube. Three hundred microliters of 1-ethyl-3-[3-dimethylaminopropyl] carbodiimide hydrochloride (EDC) and six hundred microliters of N-hydroxysulfosuccinimide (NHS) are then added to the ten milliliters of bacteria.

The glass slides are rinsed with methanol then water after soaking in the aminosilane

and placed in a clean petri dish. The bacteria, EDC and NHS mixture is then added and the dish is placed on the shaker table for at least two hours. Once the slides have been given enough time in the bacteria mixture the liquid is removed from the petri dish and disposed of in the proper receptacle. The petri dish is then set into the vacuum hood to dry for at least ten minutes. It has been found that this step is crucial to the adhesion process.

The EDC and NHS reaction targets the carboxyl groups of the LPS forming an intermediate complex [41]. When these functional groups are in contact with the aminosilane they create peptide bonds, adhering the bacteria to the glass slide. However, the groups that are exposed (not in contact with the slide) revert back to their original carboxylate form [41]. For more infomation refer to Appendix C.

3.2 Atomic Force Microscopy

The AFM measurements were done on an Asylum MFP-3D-Bio using μmasch Ultrasharp C053795 silicon nitride rectangular probes in intermittent contact mode. The manufacture reported tip height lies between $20 - 25$ μm and its given spring constant was 0.15 $\frac{N}{m}$ with a reported resonant frequency of 12 kHz. Asylum's petri dish heater was also used. (For background information regarding AFM refer to Appendix A.1.

Once the cantilever was mounted the AFM was calibrated. This was done using an unused glass slide. The InvOLS, and thermal resonant frequency was first measured followed by a manual tune. The probe then approached the glass slide and a force curve was obtained. This is to obtain a known force curve to which the force curves of the bacteria may be compared.

After calibration a drop of water was applied to the cantilever tip using a micropipette. Water was also added to the surface of the sample. The cantilever head was lowered until the drop on the cantilever formed a bridge with the water on the sample. The inverse optical lever sensitivity and thermal resonant frequency measurement was repeated as well as a manual tune. The spring constant is then changed back to the value that had been

measured in air, as that is more accurate. At this point the set point was chosen according to the amplitude and the gain was increased. The tip was brought into intermittent contact, which was determined by the change in amplitude or the point at which a chance in setpoint no longer changes the z voltage drastically. The z voltage was then centered.

The petri dish heater was connected to the environmental controller first so the Heater Panel automatically engages when the AFM software is opened. The heater and feedback were enabled and approximately ten minutes were allowed to ensure the temperature stabilized. When the deflection of the cantilever no longer drifted the temperature had stabilized. Standard imaging in fluid procedures were followed. When changing the temperature the desired parameters on the Heater Panel were entered and approximately ten minutes were given for temperature stabilization.

During the experiment bacteria were carefully chosen before performing force curves. The bacteria were chosen such that they appeared uniform, the length was in line with the scan direction, and were not attached to any other bacteria. One experiments data set was analyzed, however the same ten bacteria were analyzed at each of the temperatures, and ten force curves were done on each bacteria. The bacteria were assumed to be alive at the tie of the experiment. For more details refer to Appendix A.1.

3.3 Analysis

After each experiment, raw data files (.ibw files) were exported from the AFM software, Igor. These files were then converted to excel files using a MatLab program developed by Samantha O'Connor [61]. The converted files were then put through a second analysis program. For more information regarding the software please refer to Samantha O'Connor's paper [61].

The software imports the deflection as a function of z-sensor files converting them to force as a function of separation. Any baseline slope to the data is removed. Since the AdG model is only valid from the point of contact to where the slope in the log-log plot deviates

from $-\frac{5}{4}$ or when the cantilever's tip indents past the radius, each force curve is cropped at appropriate intervals and specified parameters as seen in schematics from Fig. 19a and 19b. The model is then fit to each curve. Variables from the model are then extracted from the model using statistical analysis. These variables include $\langle L \rangle$ and $\langle s \rangle$ as well as the standard deviation and the standard deviation of the mean values are determined [61].

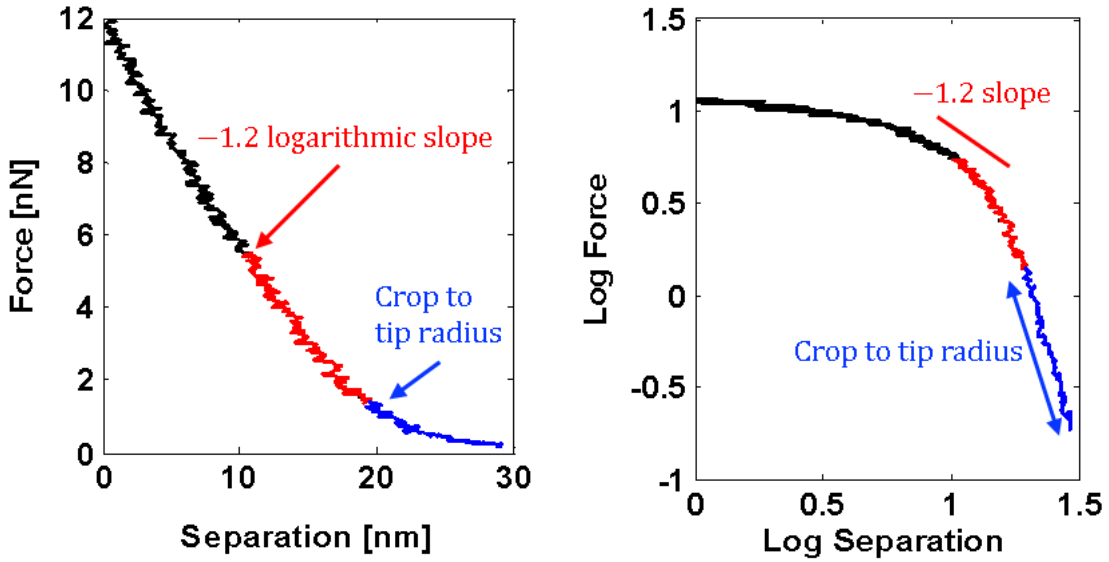

(a) Linear Force Curve

(b) Log Force Curve

Figure 19: The schematic of important cropping locations on a representative force curve in **a.)** linear scale and **b.)** Logarithmic scale. These locations are the indentation of the tip past its radius and the deviation of the $-\frac{5}{4}$ slope. [61]

The AdG model is only valid within a bounded region. These regions can be seen from the model in equation 1. The lower bound occurs at the time of contact, or when the tip of the cantilever has come into contact with the sample. Specifically, the point of contact would be when the cantilever comes into contact with the LPS.

The upper bound occurs when the tip compresses or indents past it's radius or when the logrithmic slope of the deflection deviates from the negative of the first term's exponent. In the case of the spherical tip this is $-\frac{5}{4}$. For other tip geometries see Appendix A.2. The second term is not a bound due to the separation in the numerator. If the limit $D \to 0$ is

applied that term in the equation approaches zero.

After cropping the data is then fit. Only fits with an R-squared value greater than or equal to 0.95 continue on to be analyzed. Chauvenet's criteria was used to remove outliers from the data. This criteria uses a normalized distribution of the entire set to determine outliers [61, 62]. A Welch's t-test was also used to determine significant differense. This test was chosen due to the assumption that the data would be normally distibuted but have unequal variances [63].

Chapter 4: Results and Discussion

4.1 Typical Results

A typical curve, before any analysis was done at 26 °C, is shown in Fig. 20a. A single curve is shown as deflection versus z-sensor in Fig. 20a. At large separation values, when the cantilever is far from the surface of the bacteria, the deflection is approximately constant. As the cantilever approaches the sample surface the deflection of the cantilever begins to increase, signifying an interaction between the tip of the cantilever and the surface. This same curve is seen in Fig. 20b as force versus separation. To determine the forces observed during the approach the deflection values were multiplied by the cantilever's spring constant and an offset such that the baseline force equals zero. The baseline of the approach has also been removed.

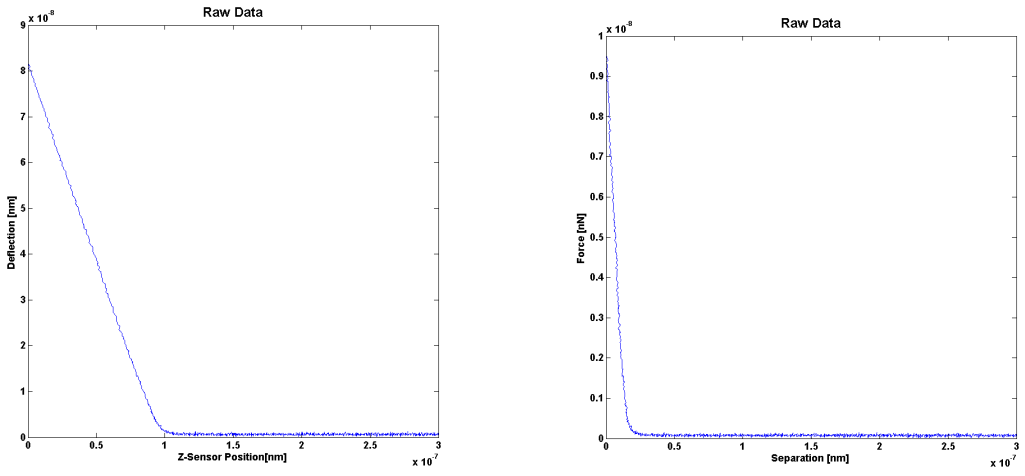

(a) Typical Deflection Curve

(b) Typical Force Curve

Figure 20: a.) The deflection of the cantilever as a function of the separation from the tip and sample surface. b.) The force of the sample on the cantilever tip as a function of the separation from the tip and sample surface.

Since the AdG model is only valid from the point of contact to where the slope in the log-log plot deviates from $-\frac{5}{4}$ or the point at which the tip indents the sample past the

radius of the tip. Figure 21 depicts the same force curve as shown in figure 20 after cropping according to the AdG model. This was done using the MatlLab program discussed in the methods chapter. It can be done manually but doing so adds a great deal of subjectivity and time to the analysis process.

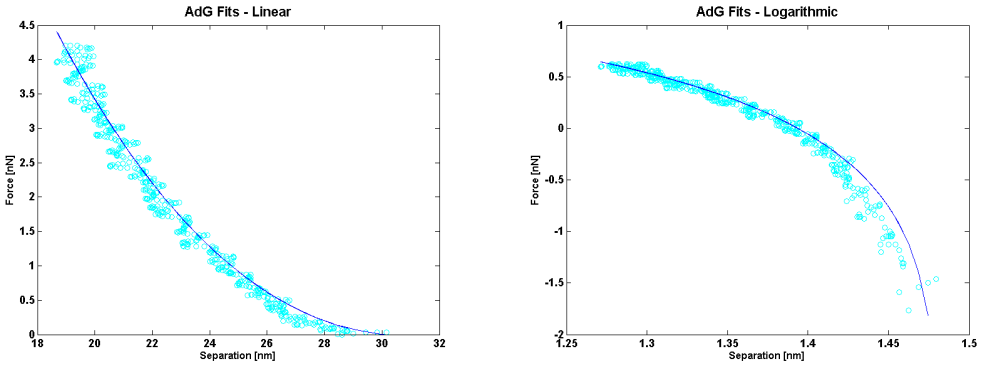

Figure 21: The force as a function of separation of a typical force curve after croping according to the AdG model.

4.2 Results as a Function of Temperature

As described in the methods, force curves were obtained at increasing temperatures at intervals of 2 °C. However, there is no data for 30 °C. This was due to the unusual resonant frequency of the cantilever measured at this temperature. The cantilever's resonant frequency may have been abormal at this temperature, due to interference from the frequency of the noise produced by the petri dish heater. Therefore the data from 30 °C was discarded.

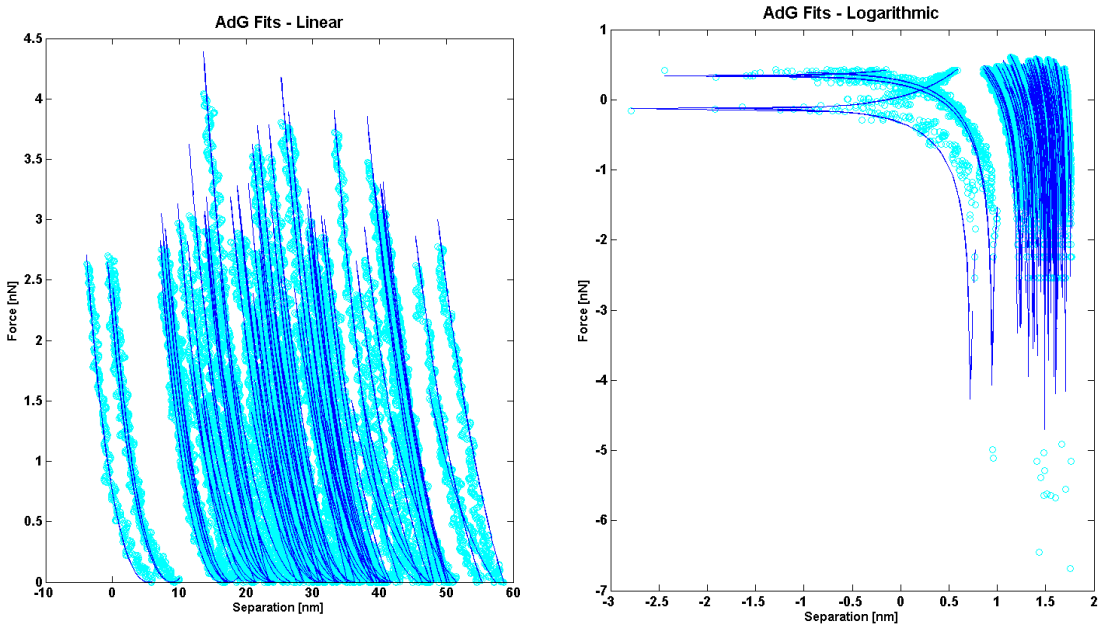

(a) Linear Scale

(b) Logarithmic Scale

Figure 22: These data were obtained at 26 °C. Only fits matching and R^2 value of 0.95 or greater are plotted (85 out of 95 possible curves). It is representative of the data obtained via the MatLab program as described in Section 3.3. The x-axis is separation measured in nanometers while the y-axis is force measured in nN. All other data can be seen in Appendix B.

These force curves were fit using the AdG model of Eq. 1 as described in the methods using the following constant parameters: minimum (coefficient of determination) R^2 value of 0.95, tip radius of 10 nm, and a spring constant of $116\frac{\text{pN}}{\text{nm}}$. The analysis and fitting was done using the MatLab program. The L and s values were determined via the model and can be found in Tables 1 and 2 corresponding to the temperatures at which the respective values were measured. The standard deviation of the mean and variance were also calculated for each variable at each temperature.

Table 1: The L values of the force curves as a function of increasing temperature obtained via methods discussed in Section 3.3. N represents the sample size of force curves used to obtain these values, SEM represents the standard deviation of the mean and SEM^2 represents the variance. The values are written in standard form. The p-value compares the L values of two temperatures.

Temperature		N	L(nm)	SEM (nm)	SEM^2 (nm^2)	p-value	
T_1	24 °C	76	57	3	9	$p_{12} = 0.03$	
T_2	26 °C	85	49.1	1.2	1.4		$p_{23} = 0.01$
T_3	28 °C	84	96	5	25	$p_{34} = 0.01$	
T_4	32 °C	84	63	3	9		$p_{45} = 0.9$
T_5	34 °C	66	64	3	9	$p_{56} = 0.01$	
T_6	36 °C	56	53.3	1.8	3.2		

Table 2: The s values of the force curves as a function of increasing temperature obtained via methods discussed in Section 3.3. N represents the sample size of force curves used to obtain these values, σ represents the standard deviation of the mean and σ^2 represents the variance. The values are written in standard form. The p-value compares the s values of two temperatures.

Temperature		N	s (nm)	SEM (nm)	SEM^2 (nm^2)	p-value	
T_1	24 °C	76	0.95	0.02	4×10^{-4}	$p_{12} = 0.01$	
T_2	26 °C	85	0.8600	0.0010	1×10^{-6}		$p_{23} = 0.01$
T_3	28 °C	84	1.10	0.02	4×10^{-4}	$p_{34} = 0.05$	
T_4	32 °C	84	1.03	0.03	9×10^{-4}		$p_{45} = 0.01$
T_5	34 °C	66	0.914	0.017	3×10^{-4}	$p_{56} = 0.5$	
T_6	36 °C	56	0.93	0.02	4×10^{-4}		

The data set was statistically analyzed with functions such as Chauvenet's criteria to ensure outliers did not skew the standard deviation [62]. A Welch's t-test was also performed

on the data to measure the signigicance of the difference between measured values at different temperatures [63]. The Welch's t-test was chosen since the values did not all have the same variance. It is assumed that the individual L and s values would follow a normal distribution given a large N value. The L and s values are also shown in Figure 23 with error bars representing the standard deviation of the mean.

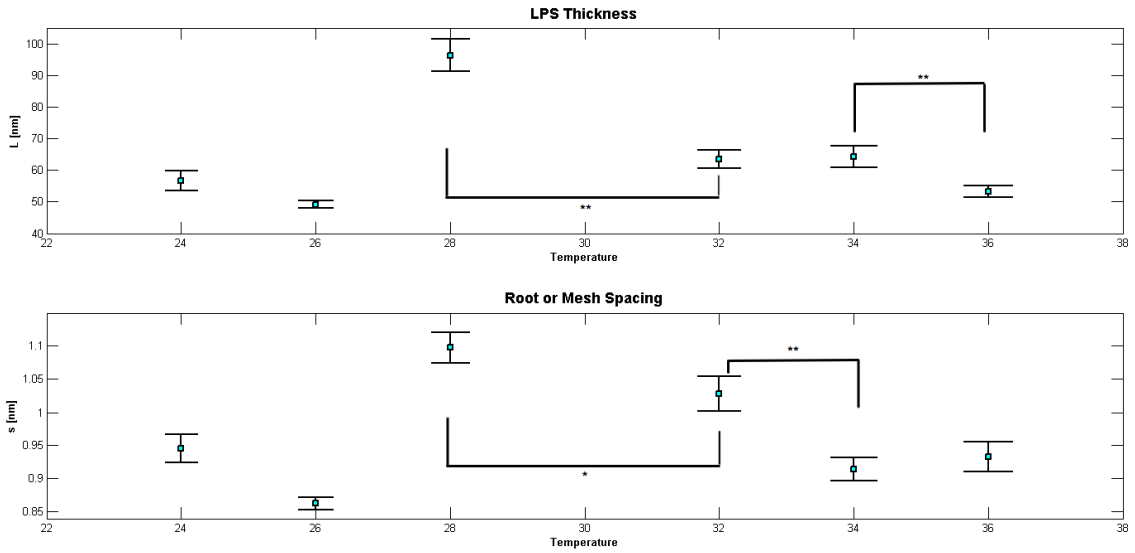

Figure 23: The average L and s values as a function of increasing temperature obtained via the MatLab program. The values seen here are the values from tables 1 and 2. The error bars represent the standard deviation of the mean. A $*$ represents a significant difference with a p-value of ≤ 0.05 and $**$ represents an extremely significant difference with a p-value of ≤ 0.01.

A positive correlation betwee the L and s values can be seen from Figure 23. The correlation coefficient was found to be 0.866. This means that as the layer of lipopolysaccharides extends (L increases) the mesh spacing would also increase. This positive correlation is what would be expected of these variables if s were the mesh spacing.

4.3 Discussion and Future Work

It was expected that L values would be on the order of several hundred nanometers, while s would be on the order of tens of nanometers or less. The obtained values of L and s both on an order of magnitude less that those previously reported. These research groups include Atabek et al. and Ivanov et al. with reported L values on the scale of several hundred nanometers and s values on the scale of tens of nanometers [11, 41].

The values for L and s in this research were obtained and analyzed with a more robust method than many previous researchers. A new AFM cantilever was used for every experiment to ensure the tip used was clean, AFM calibration was carefully executed before every experiment using a stiff sample (glass slide) in air and in liquid. The number of force curves used for analysis were large and were cropped according to the model which has not been done previously. Due the the nature of the crop over $10,000$ data points were obtained per approach curve ensuring the valid region of the curve contained enough data. The statistical analysis of the force curves and data values was both thourough as well as objective. Therefore the L and s values reported, although smaller than those previouly reported are presumed to be accuate.

However, in the majority of papers reporting on L and s, s is referred to as the root spacing or the distance between attachment points. If this was the case, then s should remain fairly constant, regardless of L or temperature change. As the data provided in the previous section the s values do not remain constant even when the L values do. The data also shows a strong positive correlation between L and s. Therefore, the data suggests that s actually represents the mesh spacing or the distance between the entanglement points. This difference can be seen in Figure 24.

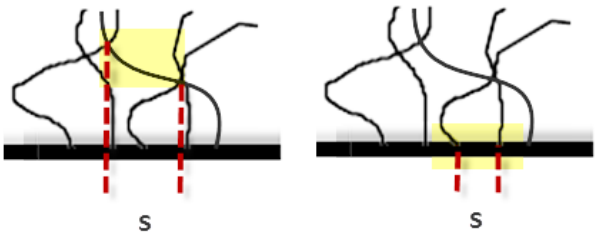

Figure 24: The schematic to distinguish between the root spacing and the mesh spacing. The left represents the mesh spacing which the right represents the root spacing.

This conclusion follows the distinction de Gennes made regarding the length parameter s when first modifying Alexander's polymer model. The distinction depended on the type of polymer adhesion. If the polymers where adsorbed onto the substrate s would represent the root spacing. However, if the polymers were not adsorbed then s would represent the mesh spacing [14]. Since the LPS can be considered terminally attached polymers rather than adsorbed polymers it would fit that s represented the mesh spacing. The data from this experiment agrees with this presumption.

Future work should still be done with this topic. The experiments and data reported in this paper should be repeated for complete assessment of accuracy and pecision. More data should be collected to determine any trend between L and s. This should be done with changing other environmental factors other than simply temperature. Some suggestions would be changes in pH, growth phase, nutrient supply, mutation type or bacterial striain, or tip radius. Future researchers should be aware that the sample preparation requires great attention to detail and patience. A suggestion before executing future research would be to try varying stiffnesses with cantilevers. The stiffness should not be so week that the tip never enters the brush but should not be so stiff as to indent into the cell membrane.

Chapter 5: Summary

Pseudomonas aeruginosa is a virulent gram negative bacteria that is very harmful to immunocompromised individuals. It is especially troublesome for cystic fibrosis and implant patients. This is due to the bacteria's ability to form micro-communities known as biofilms. These biofilms are nearly impossible to treat and in severe cases, implants must be removed. This bacteria's ability to adhere to surfaces determines the formation of the biofilm. However, the ability to adhere depends upon the lipopolysaccharides (LPS) anchored to the cell wall. Understanding how these LPS adhere is essential to preventing biofilm formation and treating bacterial infections.

An Atomic Force Microscope (AFM) was used to measure the steric forces of bacterial LPS on *Pseudomonas aeruginosa* strain 103 mutant $\Delta Wzz1$. Atomic force microscopy is a type of scanning microscopy in which a laser and photodiode are used to detect the movement of a micro-length cantilever. The forces are measured indirectly by the deflection of the cantilever and are calculated using the cantilever's spring constant. The AFM measures the steric forces, or those caused by the arrangement of the molecules and even atoms of the surface. In this case those forces are specifically due to the interaction between the probe of the cantilever and the LPS of the bacteria.

Force curves were obtained at increasing temperatures with a temperature difference of 2 °C. The data from temperature 30 °C was discarded as an unusual cantilever resonant frequency was measured. The data was analyzed using MatLab Script developed by O'Connor. The data was cropped, fit, and analyzed according to the modified version of the Alexander and de Gennes polymer model from Eq. 1.This model was originally created for two parallel substrates with polymers adhered to the interior faces. The model characterized the forces of the polymers as a function of the plate separation. However, this model can also be applied to the situation of the AFM tip and sample.

The AdG model, however, contains a density parameter, s, whose physical representation depended upon the type of adhesion of the polymers to the substrate. This parameter was

indicative of the root spacing, the distance between attachment points, for physisorbed polymers and the mesh spacing, the distance between entanglement points, for chemically adsorbed polymers. de Gennes made this distinction originally in his research yet it has not been clarified as to the physical representation of s for the LPS.

The data collected from the force curves of the AFM were a function of changing temperature. The data showed changing s and L values with changing temperature. The L and s values were on the order of magnitude previously reported by others as expected. It was concluded that due to the changing s values and the significance of those differences (measured by a Welch's t-test and p-values) s represents the mesh spacing rather than the root spacing. This also follows the distinction de Gennes made regarding the physical representation of s depending upon the polymer adhesion.

Since LPS plays a vital role in infection as well as biofilm formation it is necessary to understand the steric forces of these polysaccharides. In doing so, the forces and adhesion can be characterized leading to a better understanding of how bacteria cause infections. This will ultimately aid in developing antimicrobial treatments, antibacterial surfaces, and preventing the formation of biofilms.

References

[1] Asylum Research, 6310 Hollister Ave. Santa Barbara, CA 93117. *Petri Dish Holder and Petri Dish Heater: Installation and Operation.*

[2] Costerton J.W., S. Lewandowski, D. Caldwell, D. Korber, and G. James. MiniReview: Biofilms, the Customized Microniche. *Journal of Bacteriology*, 176(8):2137–2142, April 1994.

[3] George O'Toole, Heidi Kaplan, and Robert Kolter. Biofilm Formation As Microbial Development. *Annual Review of Microbiology*, 54:49–79, 2000.

[4] Erica Kintz, Jennifer Scarff, Antonio DiGiandomenico, and Joanna Goldberg. Lipopolysaccharide O-Antigen Chain Length Regulation in Pseudomonas aeruginosa Serogroup 011 Strain PA103. *Journal of Bacteriology*, 190(8):2709–2716, April 2008.

[5] Timothy Paustian. http://www.microbiologytext.com/index.php?module=Book&func=displayarticle
id= 60, September 2010.

[6] Van Delden Christian and Barbara H. Iglewski. Cell-to-Cell Signaling and Pseudomonas aeruginosa Infections. *Emerging Infectious Diseases [serial on the Internet]*, 4(4):551–560. wwwnc.cdc.gov/eid/article/4/4/98–0405.htm, Dec 1998.

[7] Parsek Matthew R. and Clay Fugua. Meeting Review; Biofilms 2003: Emerging Themes and Challenges in Studies of Surface-Associated Microbial Life. *Journal of Bacteriology*, 186(14):4427–4440, July 2004.

[8] Page Therapy Center. Pseudomonas aeruginosa. http://www.phagetherapycenter.com/pii/PatientServelt?command= *static_pseudomonas*, 2009.

[9] Erica Kintz and Joanna Goldberg. Regulation of lipopolysaccharide O antigen expression in Pseudomonas aeruginosa. *Future Microbiology*, 3(12):191–203, 2008.

[10] Phage Therapy Center. About Phage Therapy Center. http://www.phagetherapycenter.com/pii/PatientServelt?command=static_about&secnavpos=0&language= 0, 2009.

[11] Ivanov Ivan, Erica Kintz, Laura Porter, Joanna Goldberg, Nancy Burnham, and Terri Camesano. Relating the Physical Properties of Pseudomonas aeruginosa Lipopolysaccharides to Virulence by Atomic Force Microscopy. *Journal of Bacteriology*, 193(5):1259–1266, March 2011.

[12] Chang Debby, Nehal Abu-Lail, Farshid Guilak, Gregory Jay, and Stefan Zauscher. Conformational Mechanics, Adsorption, and Normal Force Interactions of Lubricin and Hyaluronic Acid on Model Surfaces. *Langmuir*, 24(4):1183–1193, 2008.

[13] S. Alexander. Adsorption of Chain Molecules with a Polar Head a Scaling Description. *Le Journal De Physique*, 38:983–987, 1977.

[14] de Gennes P.G. Polymers at an Interface; A Simplified View. *Advances in Colloid and Interface Science*, 27(3-4):189–209, July 1987.

[15] Hans-Jürgen Butt, Michael Kappl, Henning Mueller, Roberto Raiteri, Wolfgang Meyer, and Jürgen Rühe. Steric forces measured with the atomic force microscope at various temperatures. *Langmuir*, 15(7):2559–2565, 1999.

[16] Peter Raven and George B. Johnson. *Biology*, chapter Bacteria. In Raven and Johnsonn [64], 2001.

[17] Terri A Camesano and Bruce E Logan. Probing Bacterial Electrosteric Interactions Using Atomic Force Microscopy. *Environmental Science and Technology*, 34(16):3354–3362, 2000.

[18] Prisca Schaer-Zammaretti and Job Ubbink. Imaging of lactic acid bacteria with afm—elasticity and adhesion maps and their relationship to biological and structural data. *Ultramicroscopy*, 97(1):199–208, 2003.

[19] Ovidiu Stocia, Apichai Tuanyok, Xiaowei Yao, and Manfred H. Jericho. Elasticity of Membrane Vesicles Isolated From *Pseudomonas aeruginosa*. *Langmuir*, 19:10916–10924, 2003.

[20] Giovanni Longo, Laura Marques Rio, Andrej Trampuz, Giovanni Dietler, Alain Bizzini, and Sandor Kasas. Antibiotic-induced Modifications of the Stiffness of Bacterial Membranes. *Jounal of Microbiological Methods*, 93:80–84, 2013.

[21] C. Formosa, M. Grare, E. Jauvert, A. Coutable, J.B. Regnouf de Vains, M. Mourer, R.E. Duval, and E. Dague. Nanoscale Analysis of the Effects of Antibiotics and CX1 on a *Pseudomonas aeruginosa* Multidrug-resistant Strain. *Scientific Report*, 2(575):1–9, 2012.

[22] G Longo, L Alonso-Sarduy, L Marques Rio, A Bizzini, A Trampuz, J Notz, G Dietler, and S Kasas. Rapid detection of bacterial resistance to antibiotics using afm cantilevers as nanomechanical sensors. *Nature nanotechnology*, 8(7):522–526, 2013.

[23] Centers for Disease Control and Prevention (CDC). Antibiotic resistance threats in the united states. http://www.cdc.gov/drugresistance/threat-report-2013/pdf/ar-threats-2013-508.pdf, 2013.

[24] N.I. Abu-Lail and T.A. Camesano. Polysaccharide Properties Probed with Atomic Force Microscopy. *Journal of Microscopy*, 212:217–238, April 2003.

[25] M. Gad, Arimichi Itoh, and Atsushi Ikai. Mapping Cell Wall Polysaccharides of Living Microbial Cells Using Atomic Force Microscopy. *Cell Biology International*, 2(11):697–706, 1997.

[26] Gregory Francius et. al. Stretching Polysaccharides on Live Cells using Single Molecule Force Spectroscopy. *Nature Protocols*, 4(6):939–946, 2009.

[27] D. K. Augustin et. al. Presence or Absence of Lipopolysaccharide O Antigens Affects Type III Secretion by *Pseudomonas aeruginosa*. *Journal of Bacteriology*, 189(6):2203–2209, March 2007.

[28] Joshua Strauss, Nancy Burnham, and Terri Camesano. Atomic Force Microscopy Study of the Role of LPS O-antigen on Adhesion of *E. coli*. *Journal of Molecular Recognition*, 22:347–355, 2009.

[29] Cristina Marolda, Emily Haggerty, Michael Lung, and Miguel Valvano. Functional Analysis of Predicted Coiled-Coil Regions in the *Escherichia coli* K-12 O-Antigen Polysaccharide Chain Length Determinant Wzz. *Journal of Bacteriology*, 190(6):2128–2137, 2008.

[30] Chris Whitfield and Kane Larue. Stop and Go: Regulation of Chain Length in the Biosynthesis of Bacterial Polysaccharides. *Nature Structural & Molecular Biology*, 15(2):121–123, 2008.

[31] Sokolov Igor, Swaminathan Iyer, Venkatesh Subba-Rao, Ravi Gaikwad, and Craig Woodworth. Detection of Surface Brush on Biological Cells in Vitro with Atomic Force Microscopy. *Applied Physics Letters*, 91(2):1–3, 11 July 2007.

[32] Charlotte Perrett and Daoguo Zhou. Type Three Secretion System Effector Translocation: One Step or Two? *Cellular and Infection Microbiology*, 2(50):1–2, 2011.

[33] Sarah Daniell et. al. The Filimentous Type III Secretion Translocon of Enteropathogenic *Escherichia coli*. *Cellular Microbiology*, 3(12):865–871, 2001.

[34] Samia Dhahri, Michel Ramonda, and Christian Marlière. In-situ determination of the mechanical properties of gliding or non-motile bacteria by atomic force microscopy under physiological conditions without immobilization. *PloS one*, 8(4):e61663, 2013.

[35] Annika Gillis, Vincent Dupres, Jacques Mahillon, and Yves F Dufrêne. Atomic force microscopy: A powerful tool for studying bacterial swarming motility. *Micron*, 43(12):1304–1311, 2012.

[36] Astrid Roosjen et. al. Baterial Factors Influencing Adhesion of *Pseudomonas aeruginosa* Strains to a Poly(ethylene Oxide) Brush. *Journal of Microbiology*, 152:2673–2682, 2006.

[37] Gerda M Bruinsma et. al. Effects of Cell Surface Damage on Surface Properties and Adhesion of *Pseudomonas aeruginosa*. *Jounal of Microbiological Methods*, 45:95–101, 2001.

[38] Loredana S Dorobantu, Subir Bhattacharjee, Julia M Foght, and Murray R Gray. Analysis of force interactions between afm tips and hydrophobic bacteria using dlvo theory. *Langmuir*, 25(12):6968–6976, 2009.

[39] Peter C Y Lau, John R Dutcher, Terry J Beveridge, and Joseph S Lam. Absolute Quantition of Bacterial Biofilm Adhesion and Viscoelasticity by Microbead Force Spectroscopy. *Biophysical Journal*, 96:2935–2948, April 2009.

[40] Ardiyan Harimawan, Aruliah Rajasekar, and Yen-Peng Ting. Bacteria Attachment to Surface- AFM Force Spectroscopy and Physiochemical Analysis. *Journal of colloid and Interface Science*, 364:213–218, 2011.

[41] Arzu Atabek and Terri Camesano. Atomic Force Microscopy Study of the Effect of Lipopolysaccharides and Extracellular Polymers on Adhesion of *Pseudomonas aeruginosa*. *Journal of Bacteriology*, 189(23):8503–8509, Dec 2007.

[42] Ekaterina S Ovchinnikova, Bastiaan P Krom, Henk J Busscher, and Henny C van der Mei. Evaluation of adhesion forces of staphylococcus aureus along the length of candida albicans hyphae. *BMC microbiology*, 12(1):281, 2012.

[43] Xiaocia Sheng, Yen Peng Ting, and Simo Olavi Pehkonen. Force Measurements of Bacterial Adhesion on Metals Using a Cell Probe Atomic Force Microscope. *Jounal of Colloid and Interface Science*, 210:661–669, 2007.

[44] Ahmed Touhami, Manfred H Jericho, Jessica M Boyd, and Terry J Beveridge. Nanoscale characterization and determination of adhesion forces of pseudomonas aeruginosa pili by using atomic force microscopy. *Journal of bacteriology*, 188(2):370–377, 2006.

[45] Loredana S Dorobantu, Subir Bhattacharjee, Julia M Foght, and Murray R Gray. Analysis of force interactions between afm tips and hydrophobic bacteria using dlvo theory. *Langmuir*, 25(12):6968–6976, 2009.

[46] Pierre Parot, Yves Dufrene, Peter Hinterdorfer, Christian Grimmelec, Daniel Navajas, Jean luc Pellequer, and Simon Scheuring. Past, Present and Future of Atomic Force Microscopy in Life Sciences and Medicine. *Journal of Molecular Recognition*, 20:418–431, 2007.

[47] Mikkel Klausen, Arne Heydorn, Paula Ragas, Lotte Lambertsen, Anders Aaes-Jørgensen, Søren Molin, and Tim Tolker-Nielsen. Biofilm formation by pseudomonas aeruginosa wild type, flagella and type iv pili mutants. *Molecular microbiology*, 48(6):1511–1524, 2003.

[48] P Lal, D Sharma, P Pruthi, and V Pruthi. Exopolysaccharide analysis of biofilm-forming candida albicans. *Journal of applied microbiology*, 109(1):128–136, 2010.

[49] Y. J. Oh et. al. Effects of Substrated on Biofilm Formation Observed by Atomic Force Micrscopy. *Ultramicroscopy*, 109:874–880, 2009.

[50] Christina Gomez-Suarez et. al. Influence of Extracellular Polymeric Substances on Deposition and Redeposition of *Pseudomonas aeruginosa* to Surfaces. *Journal of Microbiology*, 148:1161–1169, 2002.

[51] Kelly M. Colvin et. al. The Pel Polysaccharide Can Serve a Structural and Protective Role in the Biofilm MAtrix of *Pseudomonas aeruginosa*. *PLoS Pathogens*, 7(1):1–13, 2011.

[52] Benjamin J. Cooley et. al. The Extracellular Polysaccharide Pel Makes the Attachment of *P. aeruginosa* to Surfaces Symmetric and Short-ranged. *The Royal Society of Chemistry*, 9:3871–3876, 2013.

[53] Christophe Beloin, A. Roux, and Jean-Mare Ghigo. *Escherichia coli* Biofilms. *Current Topics in Microbiology and Immunology*, 322(249-289), 2008.

[54] Andrea Hanna, Michael Berg, Valerie Stout, and Anneta Razatos. Role of Capsuar Colanic Acid in Adhesion of Uropathogenic *Escherichia coli*. *Applied and Environmental Microbiology*, 69(8):4474–4481, 2003.

[55] Anneta Razatos, Yea-Ling Ong, Mukul Sharma, and George Georgiou. Molecular Determinants of Bacterial Adhesion Monitored by Atomic Force Microscopy. *National Academy of Sciences*, 95:11059–11064, 1998.

[56] Francois Ahimou, Michael J Semmens, Paige J Novak, and Greg Haugstad. Biofilm cohesiveness measurement using a novel atomic force microscopy methodology. *Applied and environmental microbiology*, 73(9):2897–2904, 2007.

[57] Hillary Taunton, Chris Toprakcioglu, Lewis Fetters, and Jacob Klein. Interactions between Surfaces Bearing End-Adsorbed Chains in a Good Solvent. *Macromolecules*, 23:571–580, 1990.

[58] Andreas Serr. Interaction Forces of Poly(styrenesulfonate)-Covered Surface Measured by Direct Force Spectroscopy, 2003.

[59] Mildred Rivera, Lawerence Bryan, Robert Hancock, and Estelle McGroarty. Heterogeneity of Lipopolysaccharides from *Pseudomonas aeruginosa*: Analysis of Lipopolysaccharide Chain Length. *Journal of Bacteriology*, 170(2):512–521, Feb 1988.

[60] Evan V. Anderson. Atomic force microscopy: Lateral-force calibration and force-curve analysis, May 2012.

[61] Samantha O'Connor, Rebecca Gaddis, Evan Anderson, Terri A. Camesano, and Nancy A. Burnham. A high throughput {MATLAB} program for automated force–curve processing using the adg polymer model. *Journal of Microbiological Methods*, 109:31–38, 2015.

[62] J. R. Taylor. *An Introduction to Error Analysis: The study of uncertainties in physical measurement*. Sausalito, CA: University of Science Books, 1997.

[63] Graeme Ruxton. The unequal variance t-test is an underused alternative to student's t-text ad the mann-whitney u test. *Behavioral Ecology*, 17(4):688–690, May 2006.

[64] Peter Raven and George B. Johnsonn, editors. *Biology*. McGraw Hill, Oxford, 2001.

[65] nanoScience. nanoScience Instruments. http://www.nanoscience.com/products/afm/technology−overview.

[66] Yves F Dufrêne. Atomic force microscopy, a powerful tool in microbiology. *Journal of bacteriology*, 184(19):5205–5213, 2002.

[67] Shaoyang Liu and Yifen Wang. Application of afm in microbiology: a review. *Scanning*, 32(2):61–73, 2010.

[68] CB Volle, MA Ferguson, KE Aidala, EM Spain, and ME Núñez. Spring constants and adhesive properties of native bacterial biofilm cells measured by atomic force microscopy. *Colloids and Surfaces B: Biointerfaces*, 67(1):32–40, 2008.

[69] C Díaz, PL Schilardi, RC Salvarezza, and M Fernández Lorenzo de Mele. Have flagella a preferred orientation during early stages of biofilm formation?: Afm study using patterned substrates. *Colloids and Surfaces B: Biointerfaces*, 82(2):536–542, 2011.

[70] Daniel Rudoy, Shelten G Yuen, Robert D Howe, and Patrick J Wolfe. Bayesian change-point analysis for atomic force microscopy and soft material indentation. *Journal of the Royal Statistical Society: Series C (Applied Statistics)*, 59(4):573–593, 2010.

[71] C. Roduit. Afm figures. *www.freesbi.chi*, 2010.

[72] J.S. Lam et. al. Ultrastructural Examination of the Lipopolysaccharides of *Pseudomonas aeruginosa* Strains and Their Isogenic Rough Mutants by Freeze-Substitution. *Journal of Bacteriology*, 174(22):7159–7167, 1992.

[73] Yumiko Abe, Pavel Polyakov, Salaheddine Skali-Lami, and Gregory Francius. Elasticity and Physico-chemical Properties During drinking Water Biofilm Formation. *Biofouling*, 27(7):739–750, 2011.

[74] nanoScience Instruments. Atomic Force Microscopy. http://www.nanoscience.com/education/afm.html.

[75] Simcha Frieda Udwin. Paul Hansma Research Group. http://hansmalab.physics.ucsb.edu/afmhistory.html.

Appendices

A Supplemental Background

A.1 Atomic Force Microscopy

The atomic force microscope was developed as a new type of scanning tunneling microscope (STM), but quickly became an independent technique in the late $1980's$. It was developed by Binnig, Quate, and Gerber in 1985, to overcome the largest draw back of STM. This disadvantage was that STM could only be used on conducting samples or semiconducting surfaces [65].

The AFM, in principle, is very basic. It utilizes a cantilever, which has a very sharp tip attached to one side, a laser, and a photodiode seen in Fig. 25a. The photodiode is broken into four quadrants as seen in Fig. 25b. A laser shines onto the top of the cantilever reflecting on to a photodiode, which measures voltage changes. When a cantilever's tip is brought into contact with some substrate it traces the surface moving back and forth over the substrate. The tip and subsequently the cantilever, will move up with taller features and down with holes or shorter features. When the cantilever moves up and down the laser on the photodiode does the same, thus the sum of quadrants 1 and 2 will be greater or less than the sum of quadrants 3 and 4. Any lateral movement of the cantilever would be indicated by differences in the sum of quadrants 2 and 3 and the sum of quadrants 1 and 4. Finally the computer software translates this voltage difference into a topography image.

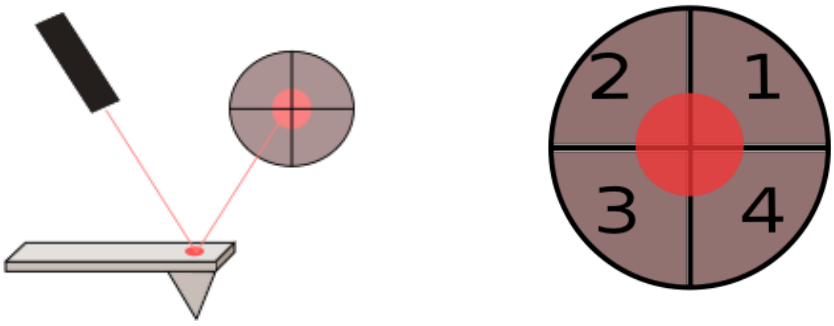

(a) AFM Duagram (b) Photodiode Division

Figure 25: Schematic of the basic principles of the AFM

Topography images, although helpful, only give insight into the surface structure rather

than any properties of the object. Utilizing Hook's law, information regarding the substrate can be obtained. Hook's law characterizes the force of the cantilever on the tip, however due to action and reaction forces the force of the substrate on the tip will be equal in magnitude but opposite in direction to the force of the tip on the substrate. Figure 26 is a free body diagram depicting the action and reaction forces of a cantilever and tip in the presence of a repulsive and attractive force. The dashed lines represent the forces of the cantilever on the tip, $\vec{F}_{cont}$ and the forces of the tip on the sample $\vec{F}_{tons}$. The two force regimes (attractive or repulsive) can be related to the bend of the cantilever. When the forces are attractive, the cantilever bends towards the sample. The opposite is true for repulsive forces.

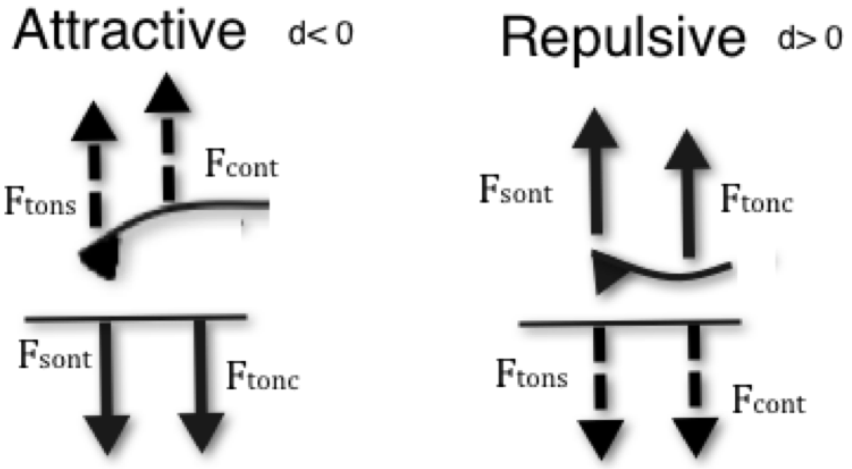

Figure 26: The free body diagram of the tip and surface forces. $\vec{F}_{cont}$ represents the force of the cantilever on the tip, $\vec{F}_{sont}$ represents the force of the sample on the tip, $\vec{F}_{tonc}$ represents the force of the tip on the cantilever and $\vec{F}_{tons}$ represents the force of the tip on the sample.

The distance a cantilever bends, $\vec{d}$, known as the deflection of the cantilever, directly relates to the force on the tip. However, the cantilever stiffness, k_c, is also very important. A stiffer cantilever will require a greater force to deflect, while a weaker cantilever will take very little force to deflect. Thus the force, according to hooks law of the cantilever on the tip, is related both to the spring constant and the deflection as seen in Eq. 2.

$$\vec{F}_{cont} = -k_c\vec{d} \tag{2}$$

However, the force of the substrate on the tip will be opposite in direction to that of the cantilever on the tip, as seen in Fig. 26. Therefore, it is more appropriate to write the equation, as seen in Eq. 3. Since the force is a vector, the direction of the force is

very important. The spring constant is intrinsically a positive value; therefore the type of force (attractive or repulsive) depends on the deflection of the cantilever. Using standard conventions, the coordinates for the deflection of the cantilever is positive if the deflection is in the positive $\hat{z}$ direction resulting in a negative or repulsive force.

$$\vec{F}_{sont} = k_c \vec{d} \tag{3}$$

Due to the ability to obtain information on the substrate as well as the topographical structure, the AFM became a powerful tool in science. However, early on in the development of the AFM only one imaging mode was available. This mode was known as contact. Much like the name implies, the tip remained in contact with the sample throughout the imaging process.

Due to the constant contact of the tip, very elastic or viscoelastic substances could not be analyzed. Although Andreas Engel made the first biological observation using the AFM in 1991, just shortly after the microscope's development, its limitations made using AFM in biology disadvantageous. The tip would often stick to the substrate making data acquisition very difficult if not impossible [46].

It was not until vibrating air, altering current or tapping mode, was developed in 1993 that it was used at all in bioscience. This mode allowed the imaging of biological substances, without damage to the substrate and at extremely high resolution. As techniques were perfected, it allowed image and data acquisition to take place in liquid. This was first done in 1995. As breakthroughs in high-speed AFM and various control techniques were developed, its use in this field became more and more prominent [46, 75].

A.2 Alexander and de Gennes Model

Alexander and de Gennes created the theoretical model based on two plates separated by a distance D and grafted with polymers whose layer thickness was L. Figure 27 depicts this theoretical system [13].

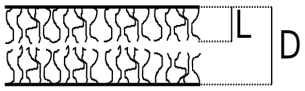

Figure 27: Alexander and de Gennes theoretical system which was used to develop the mathematical model. The system consists of two plates seprated by a distance D with a layer L of grafted polymers on each.

The original equation was a function of L, the layer thickness, D, the separation, s the root or mesh spacing depending upon polymer attachment, and T, the temperature. If had the following form

$$P(D) = \frac{k_B T}{s^3}\left[\left(\frac{2L}{D}\right)^{\frac{9}{4}} - \left(\frac{D}{2L}\right)^{\frac{3}{4}}\right] \tag{4}$$

This equation has been modified to a force equation for the AFM system, in which a tip (of different geometries), separated from the sample by a distance D, comes into contact with a layer L of polymers. Figure 28 describes this system [60].

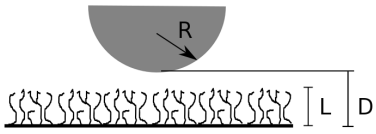

Figure 28: Atomic force microscopy system. The system consists of an AFM tip of radius R seprated by a distance D with a layer L of grafted polymers on the substrate.

The force equation has the following form for a spherical tip,

$$F_s(D) = \frac{8\pi k_B T R L}{35 s^3}\left[7\left(\frac{L}{D}\right)^{\frac{5}{4}} + 5\left(\frac{D}{L}\right)^{\frac{7}{4}} - 12\right], \tag{5}$$

and

$$F_c(D) = \frac{32\pi k_B T L^2}{385 s^3}\tan^2(\theta)\left[77\left(\frac{L}{D}\right)^{\frac{1}{4}} + 33\left(\frac{D}{L}\right) - 5\left(\frac{D}{L}\right)^{\frac{11}{4}} - 105\right] \tag{6}$$

for a conical tip and the following for a pyramidal tip

$$F_p(D) = \frac{128\pi k_B T L^2}{385 s^3}\tan^2(\theta)\left[77\left(\frac{L}{D}\right)^{\frac{1}{4}} + 33\left(\frac{D}{L}\right) - 5\left(\frac{D}{L}\right)^{\frac{11}{4}} - 105\right]. \tag{7}$$

B Complete Data Set

B.A MatLab data Plot for 24 °C

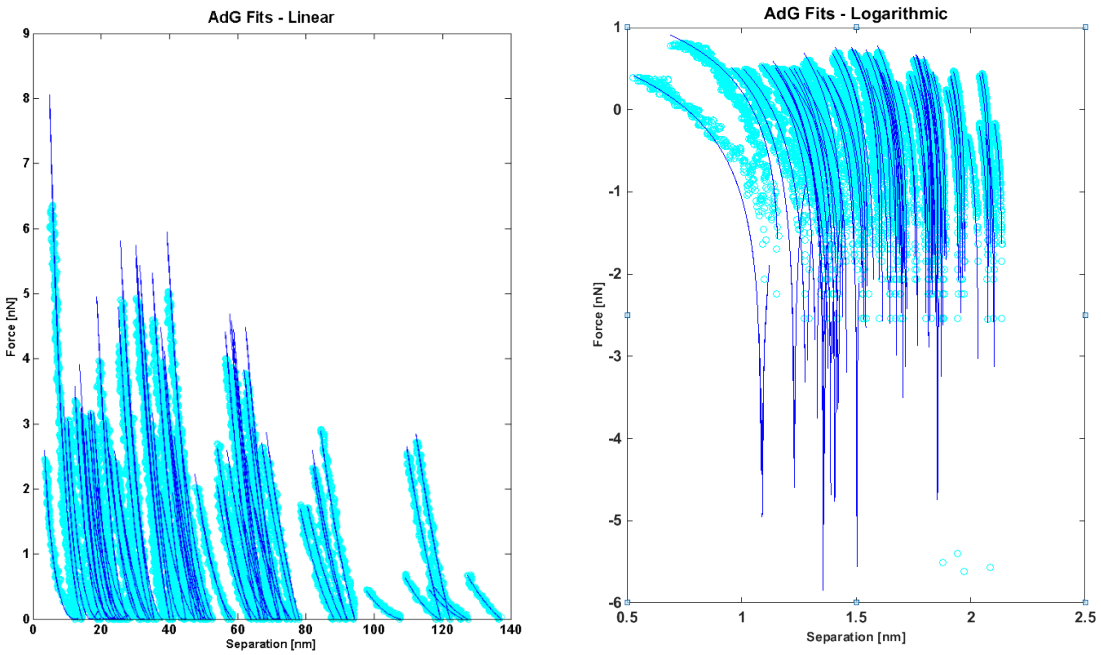

(a) Linear Scale

(b) Logarithmic Scale

Figure 29: These data were obtained at 24 °C. Only fits matching and R^2 value of 0.95 or greater are plotted (76 out of 101 possible curves). It is representative of the data obtained via the MatLab program as described in Section 3.3. The x-axis is separation measured in nanometers while the y-axis is force measured in nanonewtons. ($L = (57 \pm 3)$ nm, $s = (0.95 \pm 0.02)$ nm)

B.B MatLab data Plot for 26 °C

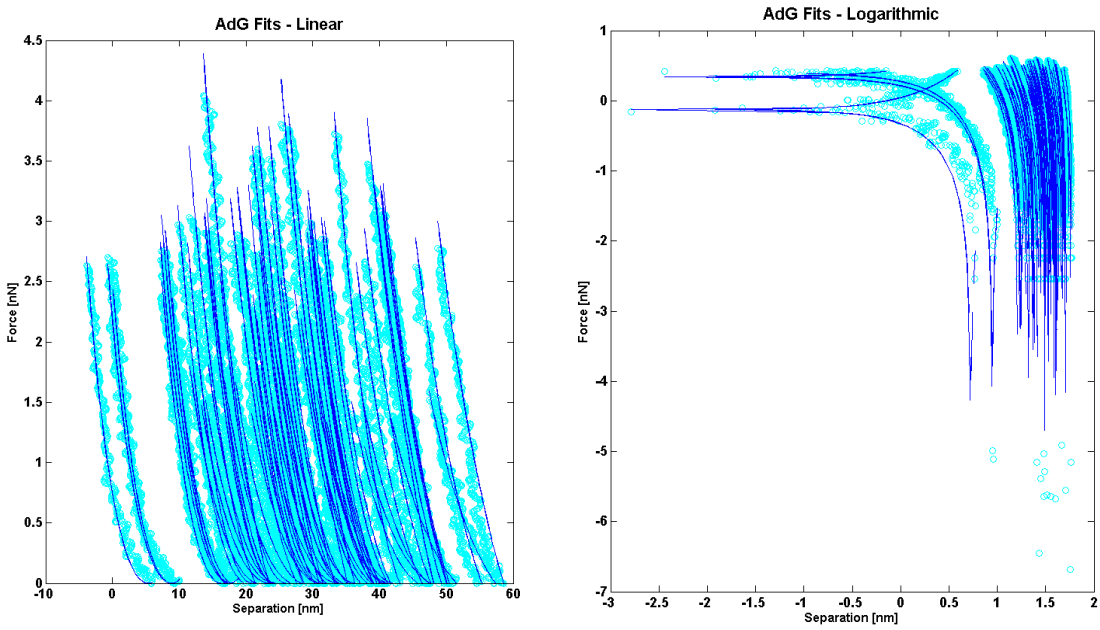

(a) Linear Scale

(b) Logarithmic Scale

Figure 30: These data were obtained at 26 °C. Only fits matching and R^2 value of 0.95 or greater are plotted (85 out of 95 possible curves). It is representative of the data obtained via the MatLab program as described in Section 3.3. The x-axis is separation measured in nanometers while the y-axis is force measured in nanonewtons. ($L = (49.1 \pm 1.2)$ nm, $s = (0.8600 \pm 0.0010)$ nm)

B.C MatLab data Plot for 28 °C

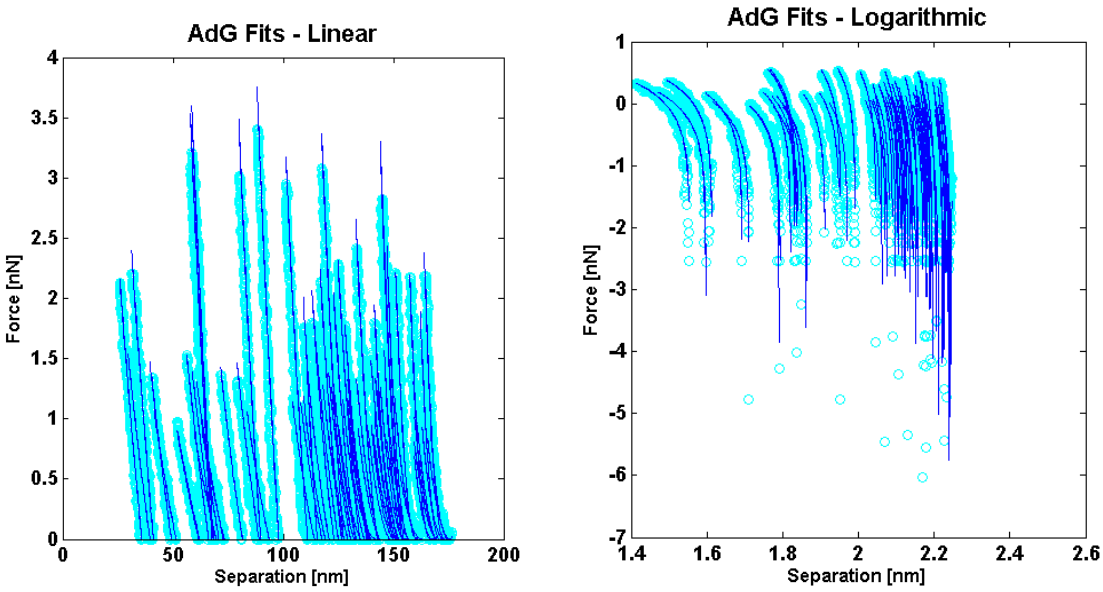

(a) Linear Scale

(b) Logarithmic Scale

Figure 31: These data were obtained at 28 °C. Only fits matching and R^2 value of 0.95 or greater are plotted (84 out of 100 possible curves). It is representative of the data obtained via the MatLab program as described in Section 3.3. The x-axis is separation measured in nanometers while the y-axis is force measured in nanonewtons. ($L = (96 \pm 5)$ nm, $s = (1.10 \pm 0.02)$ nm)

B.D MatLab data Plot for 32 °C

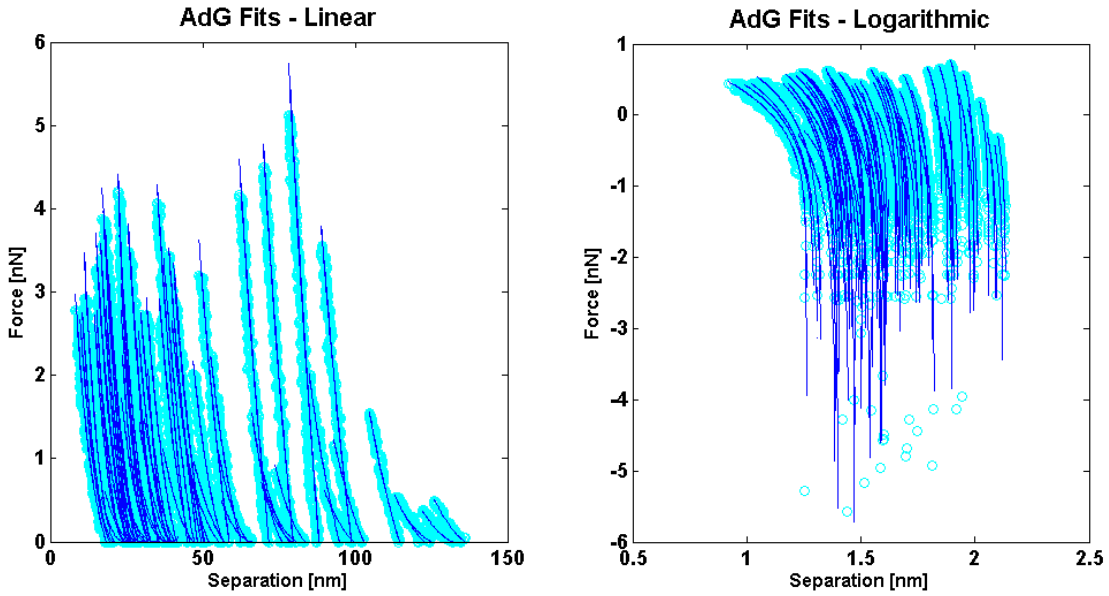

(a) Linear Scale

(b) Logarithmic Scale

Figure 32: These data were obtained at 32 °C. Only fits matching and R^2 value of 0.95 or greater are plotted (84 out of 111 possible curves). It is representative of the data obtained via the MatLab program as described in Section 3.3. The x-axis is separation measured in nanometers while the y-axis is force measured in nanonewtons. ($L = (63 \pm 3)$ nm, $s = (1.03 \pm 0.03)$ nm)

B.E MatLab data Plot for 34 °C

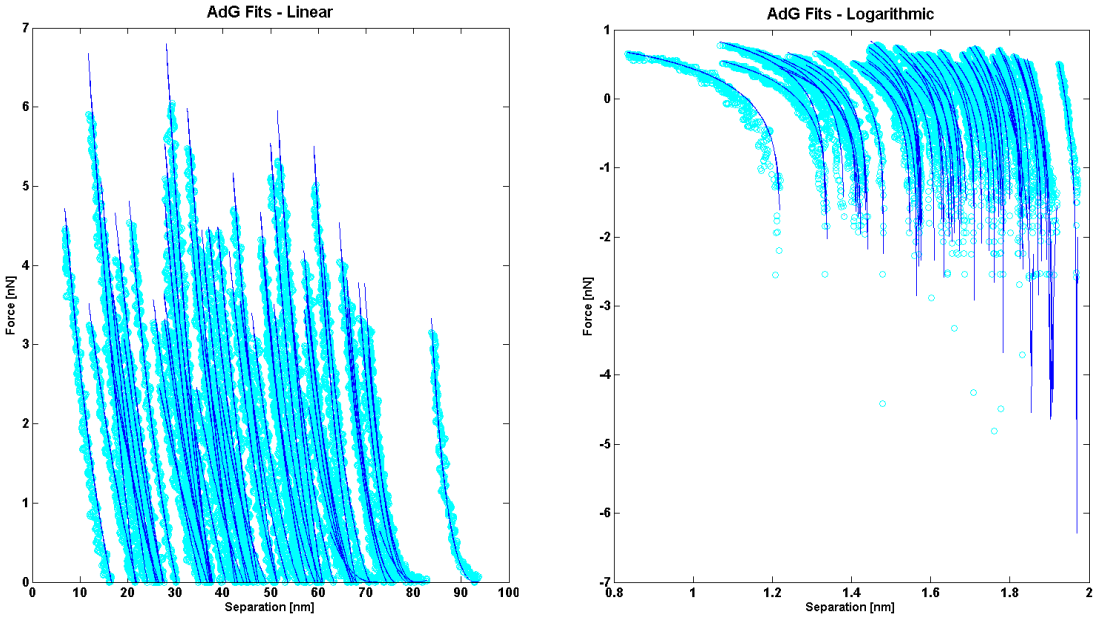

(a) Linear Scale

(b) Logarithmic Scale

Figure 33: These data were obtained at 34 °C. Only fits matching and R^2 value of 0.95 or greater are plotted (66 out of 91 possible curves). It is representative of the data obtained via the MatLab program as described in Section 3.3. The x-axis is separation measured in nanometers while the y-axis is force measured in nanonewtons. ($L = (64 \pm 3)$ nm, $s = (0.914 \pm 0.017)$ nm)

B.F MatLab data Plot for 36 °C

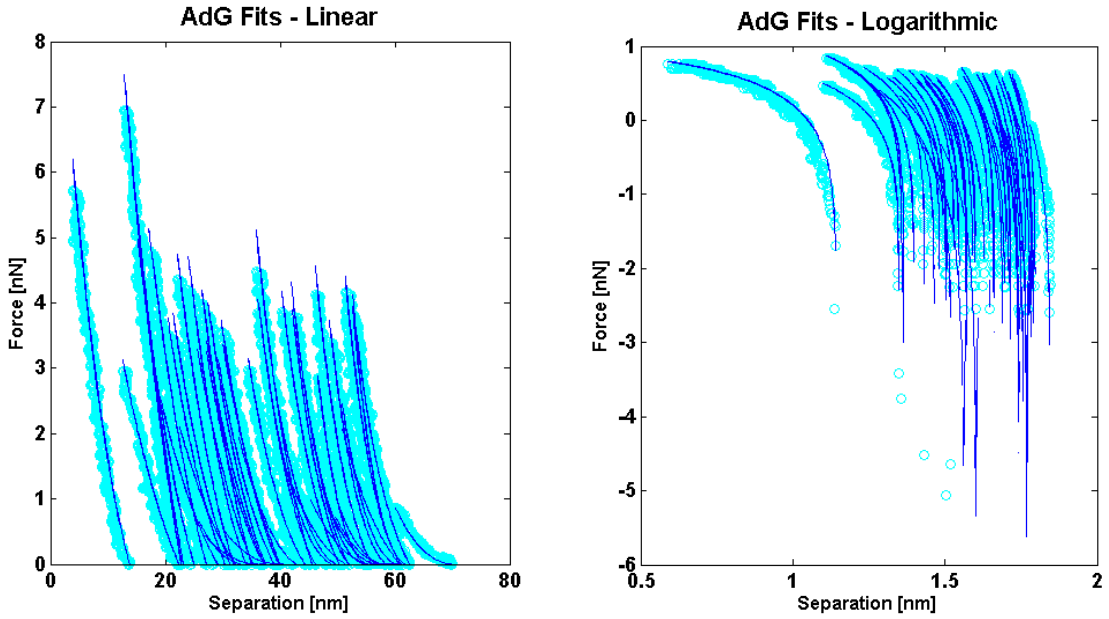

(a) Linear Scale

(b) Logarithmic Scale

Figure 34: These data were obtained at 36 °C. Only fits matching and R^2 value of 0.95 or greater are plotted (56 out of 101 possible curves). It is representative of the data obtained via the MatLab program as described in Section 3.3. The x-axis is separation measured in nanometers while the y-axis is force measured in nanonewtons.($L = (53.3 \pm 1.8)$nm, $s = (0.93 \pm 0.02)$ nm)

C Sample Preparation

C.A Cleaning Glass Slides

1. Use glass cover slips.
2. Wash slides with DI water.
3. Add slides to 2% RBS solution, enough such that the slides are covered.
4. Sonicate slides for 10 minutes.
5. Wash slides with DI water (at least 5 times).
6. Wash slides with Ethanol.

C.B LB Broth

1. Combine LB Broth with clean water using $25\frac{g}{L}$.
   a. Use 500 ml and 12.5 g
   b. Use Ultra Clear Water
2. Heat and stir at about $300°C$ until the LB is completely dissolved.
3. Autoclave using liquid cycle #2 (about 1 hour). This sterilizes the broth and container.

C.C LB Agar Plates

1. Combine LB Agar with clean water using 0.7 g per 20 mL (20 mL for each plate) in a flask.
   a. Make 60 ml with 2.1 g.
2. Stir with magnetic stir bar on a hotplate at about 300° C until the mixture begins to smoke.
   a. Watch carefully.
   b. When smoke can be seen it is done.
   c. Needs to go into Autoclave before it solidifies

3. Autoclave using liquid cycle #2 (about 1 hour).

   a Put Autoclave tape over aluminum foil of flasks.

      i. Be sure the tape is autoclave tape. It indicates whether the autoclave procedure has occured

      ii. Make sure caps are not on too tight

   b Transport glass in brown box

   c Press Button Twice

   d Sign in on clip board

4. Pour LB Agar into Petri dishes (20 mL for each plate) and let sit for about 1 hour.

5. Seal with Parafilm for later use or plate bacteria for growth.

C.D Growing Bacteria

1. Pour 50 mL of LB Broth into a glass flask under a sterile vacuum hood.

2. Proceed to a) if growing from stock, and b) if growing from plates.

   a. Take the appropriate vial of bacteria from the $-80°$C freezer and add it to the LB broth.

   b. Scrape the plate with an inoculation loop until a pellet of bacteria fills the loop. Then shake the pellet off into the LB broth.

3. Place the flask in an incubator for desired growth time (author typically used $10 - 13$ hours).

C.E Plating Bacteria

1. Grow bacteria and have agar plates ready. From left to right: incubation loops, Spirit Burner, LB Broth, Sterile Flask.

2. Stir inoculation loop in bacterial solution in order to form a meniscus in the loop (under sterile hood).

3. Wipe loop across the surface of the agar plate as much as desired.

4. Use Parafilm to seal plate.

5. Place plates with bacteria-side facing down in 37° C room.

6. Place plates in refrigerator once bacteria have grown sufficiently (about $10 - 15$ hours for the author).

C.F Making EDC

1. Combine 0.096 g of EDC with 5 mL clean water.

2. Lower pH of EDC solution to between 5 and 6 using diluted sulfuric acid (H_2SO_4).

   a. Best at 5.5

3. Store in refrigerator (lasts about one week).

C.G Making NHS

1. Combine 0.0435 g of NHS with 5 mL clean water.

2. Raise pH of NHS solution at least 10 using sodium hydroxide (NaOH), and then lower pH to between 7 and 8 using additional NHS (once the pH gets near 7, it will quickly approach 12 or so making it difficult to not surpass the $7 - 8$ range, but this is okay and possibly even necessary).

   a. Use NHS to go back down in pH.

3. Store in refrigerator (lasts about one month).

C.H The Binding Procedure

1. After growing, pour 10 mL of bacteria into each of two centrifuge tubes and centrifuge on level 7 for 10 minutes.

2. Rinse clean slides in methanol under the hood.

3. After first centrifuge cycle is done, pour out liquid from centrifuge tubes without losing bacteria and add 10 mL of water.

4. Disperse the bacteria in water using a transfer pipette and centrifuge again.

5. Add 3 : 7 ratio of 3-Aminopropyltrimethoxysilane:methanol to a new centrifuge tube under the hood and mix using the mini vortexer.

6. Pour aminosilane solution onto glass slides and leave covered for at least 20 minutes under the hood.

7. Repeat steps $2 - 4$.

8. After third centrifuge cycle is complete, pour out the water as described before, but add only 5 mL of water to each tube.

9. Disperse the bacteria in each tube and combine into one.

10. Add 300μ L EDC and then $600\mu L$ NHS to bacteria solution and tilt tube back and forth during remaining steps if possible.

11. Rinse the slides with methanol then water and add to new Petri dish after at least 20 minutes has passed since adding aminosilane (under the hood).

12. Pour bacteria solution onto slides and shake on the shaker table for at least 2 hours before imaging. This allows the bacteria to adhere to the surface evenly rather than forming colony-like sections.

13. Remove excess fluid from the petri dish and dry before imaging.

D Petri Dish Heater

D.A Installation

D.A.1 XY Hysteresis Measurement [1]

Before Changing Plate: Measure XY scanner hysteresis (piezos and mechanical assembly)

1. Open the **Test Panel**.
    a. **Note**:This is done off the surface without a tip or sample and scanner head off of the stage
    b. Click the **Programming** drop down menu then **Load Test Procedures**
    c. Select the **Testing** drop down menu then **Test Panel**
2. On the **3D Test Panel**, select the **Calibration** tab and enter the following parameters.
    a. In the Channel field: X-axis
    b. In the Action field: Measure Hysteresis.
    c. Frequency: 1.0 Hz
    d. Cycles: 50
        i The Piezo will cycle 50 times through three voltage ranges; 160 V, 10 V, and 1 V
3. Then click **Start** button
    a. A graph of LVDT sensor signal Vs. piezo drive voltage will appear.
    b. Wait for LVDT range to stabilize (50 cycles).
4. Then click **Start** again (done twice to ensure accurate results).
5. Repeat the procedure for Y-axis (channel).
    a. The X and Y hysteresis values should be as follows: $\leq 5\%$for 160 V, $\leq 4\%$ for 10 V and $\leq 3\%$ for 1 V.
    b. Typical the Y channel values are greater than X.
    c. Record value to ccompare to the values obtained after heater is installed.

D.A.2 Changing the Plate

1. The scanning head should have been removed in the previous section. If it is not remove it now.
2. Unplug the connector and remove the spring controlling the stage (y translation).
3. Using a .050 inch allen wrench remove (4) screws and washers holding the sample plate. The screws are located at the back of the stage.
4. Clean water shield and exposed stage with cotton swab and alcohol as needed.
5. Turn stage upside down such that the screw holes are facing you.
   a. Position petri dish holder/heater beneath scanner and align holes.
   b. Start all 4 screws then tighten in a diagonal pattern.
   c. Be careful not to over tighten.
   d. Re-position stage with new plate.
6. Retest X and Y scanner hysteresis.
   a. If the three hysterisis values are not similar to the previous values then the plate is most likely touching scanner.
   b. Re-position plate and re-do hysteresis.
7. After hysteresis testing is complete place scanner back onto stage and re-attach y translation spring and plug the connector back into stage.
8. Plug petri dish heater plate cable into the environmental controller (EV controller).
9. Plug the $25-25p$ interconnect cable from the environmental controller to the MFP3D controller.

D.B Using the Petri Dish Heater

1. Ensure the EV controller is on
2. Open a new template in MFP3D
   a. Heater panel window should automatically appear.
   b. If it does not see page 13 of the Petri Dish Holder and Heater manual, found on the AFM Lab computer desktop under "manuals" and at www.AsylumResearch.com.

3. Turn on the heater by selecting "on" for the following:
    a. Feedback
    b. Heater
4. Enter desired parameter values
    a. Target temperature: this is typically 37°C for mammalian cells.
    b. Note the following phenomenon and adjust parameters as needed:
        i. The temperature sensor is located inside the sample plate therefore the measured temperature is lower than the fluid/slide temperature.
        ii. The difference between these temperatures is dependent on how well heat is coupled into bottom of the glass slide or petri dish.
    c. Ramp temperature: how quickly the sample should reach target temperature. ie for a biological sample it may be 6°C/min is typical.
5. Allow ten minutes between adjusting the target temperature and measuring or imaging. It takes at least this long for the temperature to stabilize.
6. Display the **Temp vs Time Graph**.
    a. Click on **More** located next to **Display**.
    b. Click a couple of times to bring up both axes.
        i. The temperature is on the left.
        ii. The heater output is on the right.
    c. During initial heating monitor the heater output to ensure that it doesn't reach maximum.
        i. The heater output shouldn't exceed 66% when heating to 45°C.
7. NOTE: The key to successful live cell imaging is to minimize the time that the dish or slide of cells is "sitting" on the heater plate without being imaged. It is important to have the AFM completely setup and "ready to go" once the cells are placed on the sample plate. This is due to the fluid the cells are in drying from the heater plate and the rate at which the cells die.
8. Begin capturing the Temperature data by clicking on the "More" button next to Display.

9. While the fluid temperature is stabilizing, align the laser on the back of the cantilever. Zero the deflection. You will notice that the deflection will continue to drift until the fluid temperature is stable. During this period you can also tune the cantilever if you will be imaging in AC mode.

10. Follow standard fluid imaging procedures outlined in the MFP-3D manual (Chapters 8 and 9, AC Mode and Contact Mode Imaging in Liquid).